AD-A098 331 NAVAL RESEARCH LAB WASHINGTON DC F/G 20/9
EFFECT OF DIFFERENT INITIAL CONDITIONS ON THE EVOLUTION OF THE --ETC(U)
APR 81 M J KESKINEN, S L OSSAKOW
UNCLASSIFIED NRL-MR-4490 NL

END
DATE FILMED
5-81
DTIC

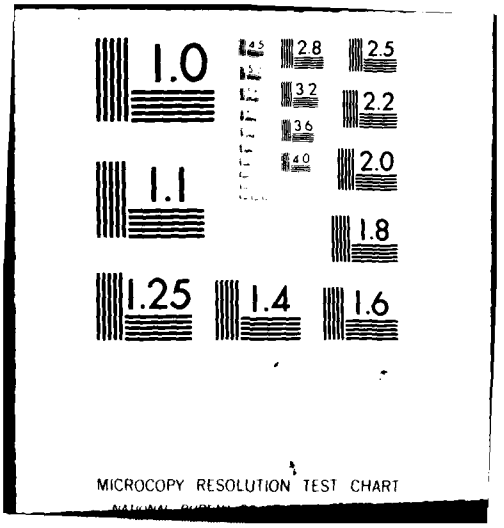
1.0
1.1
1.25
1.4
1.6
1.8
2.0
2.2
2.5
2.8
3.2
3.6
4.0
MICROCOPY RESOLUTION TEST CHART

SECURITY CLASSIFICATION OF THIS PAGE (When Data Entered)

REPORT DOCUMENTATION PAGE		READ INSTRUCTIONS BEFORE COMPLETING FORM
1. REPORT NUMBER NRL Memorandum Report 4490	2. GOVT ACCESSION NO. AD-A098 331	3. RECIPIENT'S CATALOG NUMBER
4. TITLE (and Subtitle) EFFECT OF DIFFERENT INITIAL CONDITIONS ON THE EVOLUTION OF THE E × B GRADIENT DRIFT INSTABILITY IN IONOSPHERIC PLASMA CLOUDS		5. TYPE OF REPORT & PERIOD COVERED Interim report on a continuing NRL problem. 6. PERFORMING ORG. REPORT NUMBER
7. AUTHOR(s) M.J. Keskinen and S.L. Ossakow		8. CONTRACT OR GRANT NUMBER(s)
9. PERFORMING ORGANIZATION NAME AND ADDRESS Naval Research Laboratory Washington, D.C. 20375		10. PROGRAM ELEMENT, PROJECT, TASK AREA & WORK UNIT NUMBERS 47-0889-0-1
11. CONTROLLING OFFICE NAME AND ADDRESS Defense Nuclear Agency Washington, D.C. 20305		12. REPORT DATE April 14, 1981 13. NUMBER OF PAGES 45
14. MONITORING AGENCY NAME & ADDRESS(if different from Controlling Office)		15. SECURITY CLASS. (of this report) UNCLASSIFIED 15a. DECLASSIFICATION/DOWNGRADING SCHEDULE

16. DISTRIBUTION STATEMENT (of this Report)

Approved for public release; distribution unlimited.

17. DISTRIBUTION STATEMENT (of the abstract entered in Block 20, if different from Report)

18. SUPPLEMENTARY NOTES

This research was sponsored by the Defense Nuclear Agency under Subtask S99QAXHC, work unit 00002, and work unit title "Plasma Structure Evolution."

19. KEY WORDS (Continue on reverse side if necessary and identify by block number)

Gradient drift instability
Nonlinear numerical simulations
Ionospheric plasma clouds
Different initial conditions
Power spectrum

20. ABSTRACT (Continue on reverse side if necessary and identify by block number)

The effects of different initial conditions on the evolution of the E × B gradient drift instability in large F region ionospheric plasma clouds have been studied by means of two dimensional numerical simulations. Both small and large amplitude monochromatic (one wave) and random (many waves) initial perturbations have been used to seed initially slablike plasma clouds with different magnetic field line integrated

(Continues)

DD FORM 1 JAN 73 1473 EDITION OF 1 NOV 65 IS OBSOLETE
S/N 0102-014-6601

SECURITY CLASSIFICATION OF THIS PAGE (When Data Entered)

20. ABSTRACT (Continued)

Pedersen conductivity gradient scale lengths L = 4, 6, 10 km perpendicular to the magnetic field. Independent of the initial conditions used, all of the models studied become similar in the nonlinear late time regime both in real (x, y) space and in Fourier (k_x, k_y) space where x and y define the plane perpendicular to the magnetic field. In the nonlinear regime, evidence is presented for an outer scale turnover in the one-dimensional plasma cloud conductivity spatial power spectra computed in a direction (y) perpendicular to the $\underline{E} \times \underline{B}$ drift (x) of the plasma cloud. In addition, under the different initial conditions used, the spatial power spectra in the nonlinear regime are shown to be anisotropic in the plane perpendicular to the magnetic field with most of the spectral power concentrated along and near the linearly most unstable y-direction. Furthermore, independent of the initial conditions studied, the one-dimensional x power spectra $\propto k_x^{-n_x}$ with $n_x \simeq 2$ for $2\pi/k_x$ between 1 and 80 km while the y power spectra $\propto k_y^{-n_y}$ with $n_y \simeq 2-3$ for $2\pi/k_y$ between 1 and 10 km. These quasi-final power law power spectrum states are achieved faster for the random initial perturbation than for the monochromatic initial perturbation, and similarly for the large amplitude case within each set.

CONTENTS

EFFECT OF DIFFERENT INITIAL CONDITIONS ON THE EVOLUTION OF THE E × B GRADIENT DRIFT INSTABILITY IN IONOSPHERIC PLASMA CLOUDS

1. INTRODUCTION

Experimental studies of artificially injected plasma clouds into the ionosphere [Rosenberg, 1971; Davis et al., 1974; Baker and Ulwick, 1978] have provided much information concerning not only ambient ionospheric conditions, e.g., electric and magnetic fields, but also the structure and morphology of evolving plasma clouds themselves by means of, for example, scintillation and power spectrum studies. The characteristic initial steepening, elongation, and striation of drifting plasma clouds have been explained by applying the linear theory of the ExB gradient drift instability, originally developed for laboratory plasmas [Simon, 1963], to plasma cloud geometries [Haerendel et al., 1967; Linson and Workman, 1970; Völk and Haerendel, 1971; Perkins et al., 1973]. More recently, Chaturvedi and Ossakow (1979) have studied the nonlinear stabilization of the long wavelength ExB gradient drift instability in ionospheric plasma clouds.

Numerical simulation studies [Zabusky et al., 1973; Lloyd and Haerendel, 1973; Goldman et al., 1974; Doles et al., 1976; Ossakow et al., 1975; 1977] of barium plasma clouds with a background ionosphere have reproduced not only many of the gross observational features of plasma cloud evolution, but also their spatial power spectra [Scannapieco et al., 1976], minimum scale size [McDonald et al., 1978; 1980] and outer scale size or correlation length [Keskinen et al., 1980a]. In addition numerical simulations of the local ExB gradient drift instability in ionospheric plasma clouds [Keskinen et al., 1980b] have yielded

Manuscript submitted February 3, 1981.

spatial power spectra and saturated wave amplitudes that are consistent with experiment.

However, to date, the effects of different initial conditions, i.e., changing the initial seed perturbations, on the spatial and temporal evolution of ionospheric plasma clouds have not been studied in detail. The goal of the present work is to study the effects of varying the initial conditions on the evolution of large F region initially slablike ionospheric plasma clouds both in real (x,y) space and in Fourier (k_x, k_y) space. In section 2 we present the model equations appropriate for describing large plasma clouds in the F region ionosphere. The results of the numerical solution of these equations under several different sets of initial conditions are given in sections 3 and 4. A summary and discussion of the principal results of this study are presented in Section 5.

2. MODEL EQUATIONS

For wavelengths much greater than the ion gyroradius (approximately 10 meters for Ba^+ ions in the twilight F region), the dynamics of the plasma cloud and background ionosphere can be studied in the fluid approximation [Völk and Haerendel, 1971; Perkins et al., 1973, Zabusky et al., 1973; Ossakow et al., 1975]. For large clouds (large magnetic field line integrated Pedersen conductivity compared with that of the background ionosphere), the cloud interaction with the background ionosphere (second level) can be neglected [Haerendel et al., 1967]. Furthermore, due to the very high conductivity along the magnetic field lines (typically $\sigma_p/\sigma_\parallel \sim 10^{-6}$ with σ_p and $\sigma_\parallel$ the Pedersen and parallel conductivities respectively) the field lines may be regarded as equipotentials and, as a result, a field line integrated (two-dimensional) model is justified [Völk and

and Haerendel, 1971, Perkins et al., 1973].

By adopting a Cartesian coordinate system (x,y,z) with magnetic field $B\hat{z}$, ambient electric field $E_o\hat{y}$, and after transforming to a frame drifting with velocity $\underline{V}_o = (cE_o/B)\,\hat{x}$, the two dimensional model equations for the magnetic field line integrated plasma cloud Pedersen conductivity $\Sigma(x,y)$ and the self-consistent plasma cloud electrostatic potential $\delta\Phi(x,y)$ can be written

$$\frac{\partial \Sigma}{\partial t} + \frac{c}{B}\hat{z} \times \nabla\delta\Phi \cdot \nabla\Sigma = D\,\nabla^2\Sigma \tag{1}$$

$$\nabla\cdot(\Sigma\nabla\delta\Phi) = \underline{E}_o \cdot \nabla\Sigma \tag{2}$$

where $\nabla\delta\Phi = -\underline{E}(x,y) + \underline{E}_o$, $\underline{E}(x,y,)$ the total electrostatic field, c is the speed of light, $\nabla \equiv (\partial/\partial x, \partial/\partial y)$ and D is the cross field diffusion coefficient [Perkins et al., 1973] given by $2(\nu_e/\Omega_e)(ck_B T/eB)$ with T the ion and electron temperature ν_e the sum of electron collision frequencies with cloud ions and ambient neutrals, k_B is Boltzmann's constant, and Ω_e the electron gyrofrequency. For barium plasma clouds, typical values of D lie in the range of 0.6 to 6 m^2/sec [McDonald et al., 1978]. All other symbols retain their conventional meaning. Equation (1) results from the field-line integration (along the z-direction) of the ion continuity equation while equation (2) is derived from current conservation $\nabla\cdot\underline{J}=0$.

By linearizing (1) and (2), i.e., $\Sigma = \Sigma_o + \delta\Sigma$, etc., and assuming fluctuations in magnetic field line integrated Pedersen conductivity and cloud potential $\delta\Sigma$, $\delta\Phi \propto \exp\left[i\,(k_y y + k_x x) + \gamma_{\underline{k}}\right]$ with $\underline{k}\cdot\underline{B} = 0$, $k\,L >> 1$, one finds the usual $\underline{E} \times \underline{B}$ growth rate

$$\gamma_{\underline{k}} = (cE_o/BL)(k_y/k)^2 - Dk^2 \tag{3}$$

where $k^2 = k_x^2 + k_y^2$, $L^{-1} = \partial \ln \Sigma_o/\partial x$. For cE_o/B = 100 m/sec, L = 6 km, D = 1 m^2/sec, the critical wavelength λ_c ($\gamma_{\underline{k}}$=0) ≃ 60 m.

Equations (1) and (2) can be put in dimensionless form [McDonald et al., 1978; 1980] by normalizing $\underline{x} \equiv (x,y)$, t, Σ, $\underline{V}$, $\delta\varphi$ by L_o, L_o/V_o, Σ_o, V_o, $L_o E_o$, respectively, giving

$$\frac{\partial \Sigma}{\partial t} + \hat{\underline{z}} \times \nabla \delta\varphi \cdot \nabla\Sigma = R^{-1}\nabla^2\Sigma \tag{4}$$

$$\nabla \cdot (\Sigma \nabla \delta\varphi) = \partial\Sigma/\partial y \tag{5}$$

where $R = V_o L_o/D$. As a result, the evolution of a plasma cloud is completely determined by the initial cloud configuration, boundary conditions, and the dimensionless number R.

3. NUMERICAL SIMULATIONS

Equations (1) and (2) were solved numerically on a mesh consisting of 258 grid points in the x direction ($\underline{E}_o$ x $\underline{B}$ direction) and 102 points in the y direction. With a constant grid spacing of 310 meters, the real space dimensions of the mesh were 80 km along x and 31 km along y. The magnetic field line integrated Pedersen conductivity $\Sigma(x,y)$ in (1) was advanced in time using a multi-dimensional flux-corrected variable time step leapfrog-trapezoid scheme [Zalesak, 1979] which is second order in time and fourth

order in space. At each timestep the self-consistent electrostatic potential $\delta\varphi$ due to the ion cloud was determined from (2) using a Chebychev iterative method [Varga, 1962 ; McDonald, 1980] with a convergence criterion of 10^{-4}. Periodic boundary conditions were imposed along the y direction with Neumann conditions ($\partial/\partial x = 0$) along the x direction. These boundary conditions result in a realistic representation of plasma inflow-outflow at the boundaries in the $\underline{E}_o \times B$ direction.

The principal diagnostics used to monitor the evolution of the plasma cloud are the time history of the field line integrated Pedersen conductivity of the ion cloud $\Sigma(x,y,t)$, associated spatial power spectra, and the plasma cloud electrostatic potential $\delta\varphi(x,y,t)$. These power spectra were obtained by first Fourier transforming the real space cloud Pedersen conductivity $\delta\Sigma(x,y) \rightarrow \delta\Sigma(k_x, k_y)$ where $\delta\Sigma(x,y) = \Sigma(x,y)-\Sigma_o$, Σ_o the maximum cloud conductivity. The power spectral density $|\delta\Sigma(k_x,k_y)/\Sigma_o|^2$ was then formed and the one-dimensional power spectra $P(k_x)$ and $P(k_y)$ were computed where

$$P(k_x) = \int dk_y \; |\delta\Sigma(k_x,k_y)/\; \Sigma_o|^2$$

and

$$P(k_y) = \int dk_x \; |\delta\Sigma(k_x,k_y) \; /\Sigma_o|^2$$

These transverse averaged power spectra $P(k_x)$ and $P(k_y)$ were then fitted [Keskinen et al., 1980a] with a three parameter (spectral strength $P_{o\alpha}$, spectral index n_α, and outer scale wavenumber $k_{o\alpha}$) power law of the form

$$P(k_\alpha) = P_{o\alpha} \; (1 + k_\alpha/k_{o\alpha})^{-n_\alpha/2}$$

where α = x or y. The method used to extract the best fit parameters

$P_{o\alpha}, n_\alpha, k_{o\alpha}$, is a nonlinear least squares procedure [Keskinen et al., 1980a] which computes $P_{o\alpha}$ and n_α directly and then iterates to find $k_{o\alpha}$.

Initially, the field line integrated Pedersen conductivity of the plasma cloud was taken to be of the form

$$\Sigma(x,y,t=o)/\Sigma_o=[M \exp(-x^2/L^2) + 0.1] \ (1+\varepsilon(x,y))$$

where both the mean amplitude and spatial distribution of $\varepsilon(x,y)$ were varied. In previous numerical studies [McDonald et al., 1978: 1980; Keskinen et al., 1980a] $\varepsilon(x,y)$ was given a root mean square value of 3% and generated from a randomly phased Gaussian power spectrum. In this work two different forms for $\varepsilon(x,y)$ were used. In the first case $\varepsilon(x,y) = A \cos 3 k_F y$, a single monochromatic wave along the linearly most unstable y-direction with wavelength $\lambda = 2\pi/3k_F = 10$km where $k_F = 2\pi/30\text{km}^{-1}$. In the second case, $\varepsilon(x,y) = A\,(1-2r(x,y))$ where $r(x,y)$ is a random number between 0 and 1. This case models the many wave initial condition. In both cases small and large amplitude initial perturbations were modeled by taking A equal to 0.03 and 0.15 respectively. Figure 1 gives a rough schematic plot of the structure of $\varepsilon(k_x, k_y)$ used in these simulations. For both forms and amplitudes of $\varepsilon(x,y)$, three simulations were made distinguished by different initial field line integrated cloud Pedersen conductivity scale lengths L = 4,6,10 km perpendicular to the magnetic field. For all cases V_o = 100 m/sec and the cross field diffusion coefficient $D = 1\ m^2/sec$. In addition, in all cases M = 1 so that the maximum field line integrated Pedersen conductivity of the cloud to the background ionosphere is approximately 10. For the sake of consistency and brevity, we confine ourselves to the description of the evolution of the L = 6 km

barium plasma cloud only.

4. RESULTS

Figures 2a-2d illustrate the evolution of an initially slablike barium plasma cloud driven unstable by a 3% monochromatic initial wave by showing the real space isodensity contours of the field-line integrated Pedersen cloud conductivity in the plane perpendicular to the magnetic field. Figure 2a displays the initial configuration. Figure 2b shows the plasma cloud conductivity at t = 200 sec where some elongation, steepening, and jetting to the frontside has begun. Figure 2c details the cloud structure at t = 1000 sec where the characteristic fingers have formed and stretched along the $\underline{E}_o \times \underline{B}$ drift direction. Figure 2d gives the structure in the late time nonlinear regime at t = 2400 sec (γ_{max} t≃ 40 with γ_{max} the maximum linear growth rate). Similiar shapes and morphologies are observed and for the other two Pedersen conductivity gradient scale lengths studied, i.e., L = 4 and 10 km, but on different time scales.

Figure 3 gives representative one-dimensional plasma cloud Pedersen conductivity spatial power spectra computed in the nonlinear late time (t = 2400 sec) regime both parallel $P(k_x)$ and perpendicular $P(k_y)$ to the plasma cloud drift for the 3% monochromatic initial conditions with L = 6 km. Before significant bifurcation occurs, the perpendicular power spectrum $P(k_y)$ is not described by a power law, but is dominated by the initially excited mode $k_y/k_{Fy} = 3$ where $k_{Fy} = (2\pi/30)\text{km}^{-1}$ is the fundamental mode number in the y-direction. However, due to the steep edges of the plasma cloud striations in the parallel x-direction the parallel power spectra $P(k_x)$ do conform to a power law with spectral index of approximately $n_x \simeq 2$. At

late times in the nonlinear regime, however, the perpendicular $P(k_y)$ power spectra also tend toward a power law.

Figure 4 shows the time histories of n_x and n_y for the small amplitude monochromatic initial conditions with L = 6 km. Similar results were found for L = 4, 10 km.

Figure 5 gives a sample contour plot of the unaveraged two-dimensional spatial power spectra of the plasma cloud Pedersen conductivity at t = 2400 sec using 3% monochromatic initial conditions with L = 6 km. As can be seen, the two-dimensional spatial power spectra is anisotropic with most of the spectral power concentrated along and near the linearly most unstable y-direction. This anisotropy in (k_x,k_y) space is consistent with the late time distribution in (x,y) space of the field line integrated cloud Pedersen conductivity which show striations elongated much more in the x-direction ($\underline{E}_o \times \underline{B}$ drift direction). Similar anisotropic spatial power spectra in the late time nonlinear regime are also found using the large amplitude (15%) monochromatic initial conditions.

Figures 6a-6d give the real space distribution of field line integrated cloud Pedersen conductivity for the large amplitude 15% monochromatic initial conditions for L = 6 km. Figure 6b describes the conductivity profile also at t = 200 sec and shows a similar configuration to the 3% case in Figure 2b with the exception that more elongation and jetting to the frontside has taken place in the larger amplitude case. For the monochromatic initial conditions used the evolution of the plasma cloud with the larger amplitude perturbation was found to proceed on a faster time scale than the plasma cloud seeded with a smaller amplitude perturbation. Figure 6c displays the cloud contours at t = 1000 sec while Figure 6d details the plasma cloud field line integrated Pedersen conductivity at t = 2400 sec and is not dissimilar from

the plasma cloud configuration using the 3% monochromatic initial conditions (cf. Fig. 2d). Similar morphologies are also observed for the plasma clouds with conductivity gradient scale lengths L=4,6,10 km, but on different time scales with the L=4 km case proceeding faster and the L=10 km case slower.

Figure 7 gives sample one-dimensional parallel $P(k_x)$ and perpendicular $P(k_y)$ spatial power spectra of plasma cloud conductivity computed in the nonlinear late time (t = 2400 sec) regime for 15% monochromatic initial conditions with L = 6 km. Note the similarity with Figure 3.

Figure 8 displays the time dependence of the best fit spectral indices n_x and n_y for the 15% monochromatic initial perturbation with L = 6 km. As can be noted the spectral indices n_x and n_y achieve their quasi-steady state values on a slightly faster time scale (on the order of 100-200 sec) for the larger amplitude monochromatic perturbation as opposed to the smaller amplitude monochromatic initial conditions (see Figure 4). The value for the spectral index in the $\underline{E}\times\underline{B}$ direction approaches $n_x \simeq 2$ while $n_y \simeq 2$-3. Similar spectral indices are also found for the other two cases studied, i.e., L = 4, 10 km, but again on different time scales.

Figures 9a-9d portray the evolution of the plasma cloud using purely random initial conditions with maximum amplitude of 3% for L = 6 km. In these simulations the initial evolution of a test wave is influenced not only by the ambient plasma cloud, but also by a many wave background. Figure 9b displays the cloud at t = 200 sec and shows the initial random perturbations developing on the backside. Figure 9c illustrates the field line integrated Pedersen conductivity contours at t = 1000 sec with striation and elongation evident. Figure 9d shows the cloud configuration at t = 2400 sec and is similar to the late time configurations using the monochromatic initial conditions as shown in Figure 2d and 6d. The evolution of the clouds with gradient scale lengths L = 4,10 km under 3% random initial conditions is

similar to the L = 6 km case, but on different time scales, i.e., the L = 4 km cloud structuring faster in absolute time and the L = 10 km cloud developing slower.

Figure 10 shows sample one-dimensional power spectra of plasma cloud conductivity with L = 6 km both parallel $P(k_x)$ and perpendicular $P(k_y)$ to the ExB drift (x-direction) at t = 2400 sec for the purely random 3% initial conditions. The time histories of the best fit spectral indices n_x and n_y both in the parallel $P(k_x)$ and perpendicular $P(k_y)$ directions with L = 6 km for the small amplitude (3%) random initial conditions are displayed in Figure 11. After initial transients, the spectral index in the $\underline{E}_o \times \underline{B}$ direction becomes $n_x \simeq 2$ with $n_y \cong 2\text{-}3$. In comparing the time evolution of n_x and n_y for the 3% monochromatic and random initial conditions (see Figures 4 and 11) one notes that the spectral indices reach their quasi-steady state values faster for the many wave random initial conditions. This is particularly true for the spectral index n_y. The same values for the spectral indices n_x and n_y are also observed using the gradient scale lengths L = 4,10 km starting from the 3% random initial conditions. These spectral indices are in agreement with both experimental values [Baker and Ulwick, 1978; Kelley et al., 1979] and previous one level [McDonald et al., 1980; Keskinen et al., 1980] and two-level [Scannapieco et al., 1976] numerical simulations of ionospheric barium clouds using different initial conditions.

The turnover or outer scale size in the one-dimensional perpendicular power spectra $P(k_y)$ of the plasma cloud conductivity with L = 6 km using the small amplitude (3%) random initial perturbations is plotted in Figure 12 as a function of time. In the early nonlinear regime, the perpendicular outer scale size $2\pi/k_{oy}$ approximates the initial parallel Pedersen conductivity

gradient scale length L of the cloud in agreement with previous numerical simulations [Keskinen et al., 1980a] using Gaussian initial conditions with mean amplitude of 3%.

Figure 13 shows a representative sample of the unaveraged two-dimensional spatial power spectra of the cloud Pedersen conductivity of t = 2400 sec using the 3% random initial conditions with L = 6 km. The power spectra is anisotropic with most of the power located along and near the linearly most unstable y-direction. Note the similarities with Figure 5 which evolved from monochromatic initial conditions. Similar anisotropy is found for L = 4,10 km.

Figures 14a-14d display the evolution of the barium plasma cloud using the 15% purely random initial conditions for the L = 6 km scale length. Comparing the plasma cloud structure in Figure 14b at t = 200 sec with Figure 9b (small amplitude random initial perturbation at t = 200 sec) one again notes the increased elongation and penetration to the frontside in the larger initial amplitude case. Figure 14c shows the striations at t = 1000 sec while Figure 14d illustrates further bifurcation at t = 2400 sec. Many similarities can be seen in comparing Figure 14d and Figure 9d.

Figure 15 shows sample one-dimensional power spectra of the L = 6 km plasma cloud Pedersen conductivity both parallel $P(k_x)$ and perpendicular $P(k_y)$ to the $\underline{E}\underline{x}\underline{B}$ drift (x-direction) at t = 2400 sec for the purely random 15% initial conditions. The time histories of the best fit spectral indices n_x and n_y both in the parallel $P(k_x)$ and perpendicular $P(k_y)$ directions with L = 6 km for the large amplitude (15%) random initial conditions are displayed in Figure 16. The spectral index in the $\underline{E}_o \times \underline{B}$ direction (x-direction) approaches $n_x \simeq 2$ with the spectral index perpendicular to the $\underline{E}_o \times \underline{B}$

drift $n_y \approx 2$-3. By comparing Figure 16 (15% random initial conditions) with Figure 11 (3% random initial conditions) one again notes that the spectral indices n_x and n_y approach their quasi-steady state values on a slightly faster time scale for the larger amplitude initial perturbations. In addition, in comparing Figure 16 (15% random initial conditions) with Figure 8 (15% monochromatic initial conditions) it can be said that the spectral indices n_x and n_y develop on a faster time scale for the many wave initial perturbations as opposed to the single wave monochromatic initial conditions.

The turnover or outer scale size in the one dimensional perpendicular power spectra $P(k_y)$ for the L = 6 km plasma cloud seeded with the large amplitude (15%) random initial perturbations corresponding to Figure 14 is plotted in Figure 17 as a function of time. In the nonlinear regime (for the times the simulations were run) the perpendicular outer scale size $2\pi/k_{oy}$ approximates the initial parallel (to $\underline{E}_o \times \underline{B}$ motion) Pedersen conductivity gradient scale length L of the cloud in agreement with the 3% random initial conditions (see Figure 12). Again, this scaling is achieved on a slightly faster time scale than with the smaller amplitude 3% random initial perturbations.

5. SUMMARY OF RESULTS

We have studied the effects of different initial conditions on the evolution of large F region ionospheric plasma clouds driven unstable by the $\underline{E}\times\underline{B}$ gradient drift instability. This has been accomplished by the numerical solution of the fundamental one level (one for the plasma cloud and neglect of cloud-background ionosphere interaction) two-dimensional magnetic field line integrated plasma cloud fluid equations using several different sets of initial conditions. In these numerical simulations both large and small

purely random and monochromatic initial conditions have been used to study initially slablike plasma cloud models with different magnetic field line integrated Pedersen conductivity gradient scale lengths L = 4,6,10 km perpendicular to the magnetic field. Independent of the initial condition studied, all models, in the nonlinear late time regime become similar both in real (x,v) space and in Fourier (k_x,k_v) space where x and v define the plane perpendicular to the direction of the magnetic field. In the nonlinear regime, an outer scale turnover is observed in the spatial power spectra computed in a direction (v) perpendicular to the ExB drift (x) of the plasma cloud. Under the different initial conditions studied, the two-dimensional spatial power spectra in the nonlinear regime in the plane perpendicular to the magnetic field is found to be anisotropic with most of the spectra power concentrated in the linearly most unstable v-direction. Furthermore, independent of the initial conditions used in this report the one-dimensional x power spectra is $\propto k_x^{-n_x}$ with $n_x \sim 2$ for $2\pi/k_x$ between 1 and 80 km, while the v power spectra $\propto k_v^{-n_v}$ with $n_v \sim 2$-3 for $2\pi/k_v$ between 1 and 10km. Also the random initial perturbation case achieves its quasi-final power law power spectrum description on a slightly faster time scale than the single monochromatic wave initial perturbation case. Within the context of initial perturbation amplitude, for a given case, the larger amplitude perturbation attains the quasi-final state more rapidly. These numerical results are consistent with recent experimental [Baker and Ulwick, 1978; Kelley et al., 1976; Chaturvedi and Ossakow, 1979; Keskinen et al., 1980] studies of ionospheric plasma clouds.

Future analytical and numerical studies of the evolution of ionospheric plasma clouds are planned which include the addition of inertial effects and the coupling to other ionospheric levels.

ACKNOWLEDGMENTS

We wish to thank B.E. McDonald for useful discussions. This work was supported by the Defense Nuclear Agency.

REFERENCES

Baker, K.D., and J.C. Ulwick, Measurements of Electron Density Structure in Barium Clouds, Geophys. Res. Lett., 5, 723, 1978.

Chaturvedi, P.K., and S.L. Ossakow, Nonlinear Stabilization of the E x B Gradient Drift Instability in Ionospheric Plasma Clouds, J. Geophys. Res., 84, 419, 1979.

Davis, T.N., G. J. Romick, E.M. Wescott, R.A. Jeffries, D.M. Kerr, and H.M. Peek, Observations of the Development of Striations in Large Barium Clouds, Planet. Space Sci., 22, 67, 1974.

Doles, J.J., III, N.J. Zabusky, and F.W. Perkins, Deformation and Striation of Plasma Clouds in the Ionosphere, 3, Numerical Simulations of a Multi-level Model with Recombination Chemistry, J. Geophys. Res., 81, 5987, 1976.

Goldman, S. R., S. L. Ossakow, and D.L. Book, On the Nonlinear Motion of a Small Barium Cloud in the Ionosphere, J. Geophys. Res., 79, 1471, 1974.

Haerendel, G., R. Lust, and E. Rieger, Motion of Artificial Ion Clouds in the Upper Atmosphere, Planet. Space Sci., 15, 1, 1967.

Kelley, M.C., K.D. Baker, and J.C. Ulwick, Late Time Barium Cloud Striations and Their Possible Relationship to Equatorial Spread F, J. Geophys. Res., 84, 1898, 1979.

Keskinen, M.J., B.E. McDonald, and S.L. Ossakow, Preliminary Numerical Study of the Outer Scale Size of Ionospheric Plasma Cloud Striations, J. Geophys. Res, 85, 2349, 1980a.

Keskinen, M.J., S.L. Ossakow, and P.K. Chaturvedi, Preliminary Report of Numerical Simulations of Intermediate Wavelength ExB Gradient Drift Instability in Ionospheric Plasma Clouds, J. Geophys. Res., 85, 3485, 1980b.

Linson, L.M., and J.B. Workman, Formation of Striations in Ionospheric Plasma Clouds, J. Geophys. Res., 75, 3211, 1970.

Lloyd, J.H., and G. Haerendel, Numerical Modeling of the Drift and Deformation of Ionospheric Plasma Clouds and of Their Interaction with Other Layers of the Ionosphere, J. Geophys. Res., 78, 7389, 1973.

McDonald, B.E., S.L. Ossakow, S.T. Zalesak, and N.J. Zabusky, Determination of Minimum Scale Sizes in Plasma Cloud Striations, in Effect of the Ionosphere on Space and Terrestrial Systems, edited by J.M. Goodman, U.S. Government Printing Office, Washington, D.C. 1978.

McDonald, B.E., The Chebychev Method for Solving Nonself-adjoint Elliptic Equations on a Vector Computer, J. Comput. Phys., 35, 147, 1980

McDonald, B.E., S.L. Ossakow, S.T. Zalesak, and N.J. Zabusky, Scale Sizes and Lifetimes of F Region Striations as Determined by the Condition of Marginal Stability, submitted to J. Geophys. Res., 1980.

Ossakow, S.L., A.J. Scannapieco, S.R. Goldman, D.L. Book, and B.E. McDonald, Theoretical and Numerical Simulation Studies of Ionospheric Inhomogeneities Produced by Plasma Clouds, in Effect of the Ionosphere on Space Systems and Communications, edited by J.M. Goodman, U.S. Government Printing Office, Washington, D.C. 1975.

Ossakow, S.L., S.T. Zalesak, and N.J. Zabusky, Recent Results on Cleavage, Bifurcation, and Cascade Mechanisms in Ionospheric Plasma Clouds, Memo. Rep. 3579, Nav. Res. Lab., Washington, D.C., Aug., 1977.

Perkins, F.W., N.J. Zabusky, and J.H. Doles III, Deformation and Striation of Plasma Clouds in the Ionosphere, 1, J. Geophys, Res., 78, 697, 1973.

Rosenberg, N.W., Observations of Striation Formation in a Barium Ion Cloud, J. Geophys. Res., 76, 6856, 1971.

Scannapieco, A.J., S.L. Ossakow, S.R. Goldman, and J.M. Piere, Plasma Cloud Late Time Striation Spectra, J. Geophys. Res., 81, 6037, 1976.

Simon, A., Instability of a Partially Ionized Plasma in Crossed Electric and Magnetic Fields, Phys. Fluids, 6, 382, 1963.

Varga, R.S. Matrix Iterative Analysis, Prentice Hall, Englewood Cliffs, N.J. 1962.

Völk, H.J., and G. Haerendel, Striations in Ionospheric Ion Clouds, 1, J. Geophys. Res., 76, 4541, 1971.

Zabusky, N.J., J.H. Doles III, and F.W. Perkins, Deformation and Striation of Plasma Clouds in the Ionosphere, 2, Numerical Simulation of a Non-linear Two-dimensional Model, J. Geophys. Res., 78, 711, 1973.

Zalesak, S.T., Fully Multidimensional Flux-corrected Transport Algorithms for Fluids, J. Comp. Phys., 31, 335, 1979.

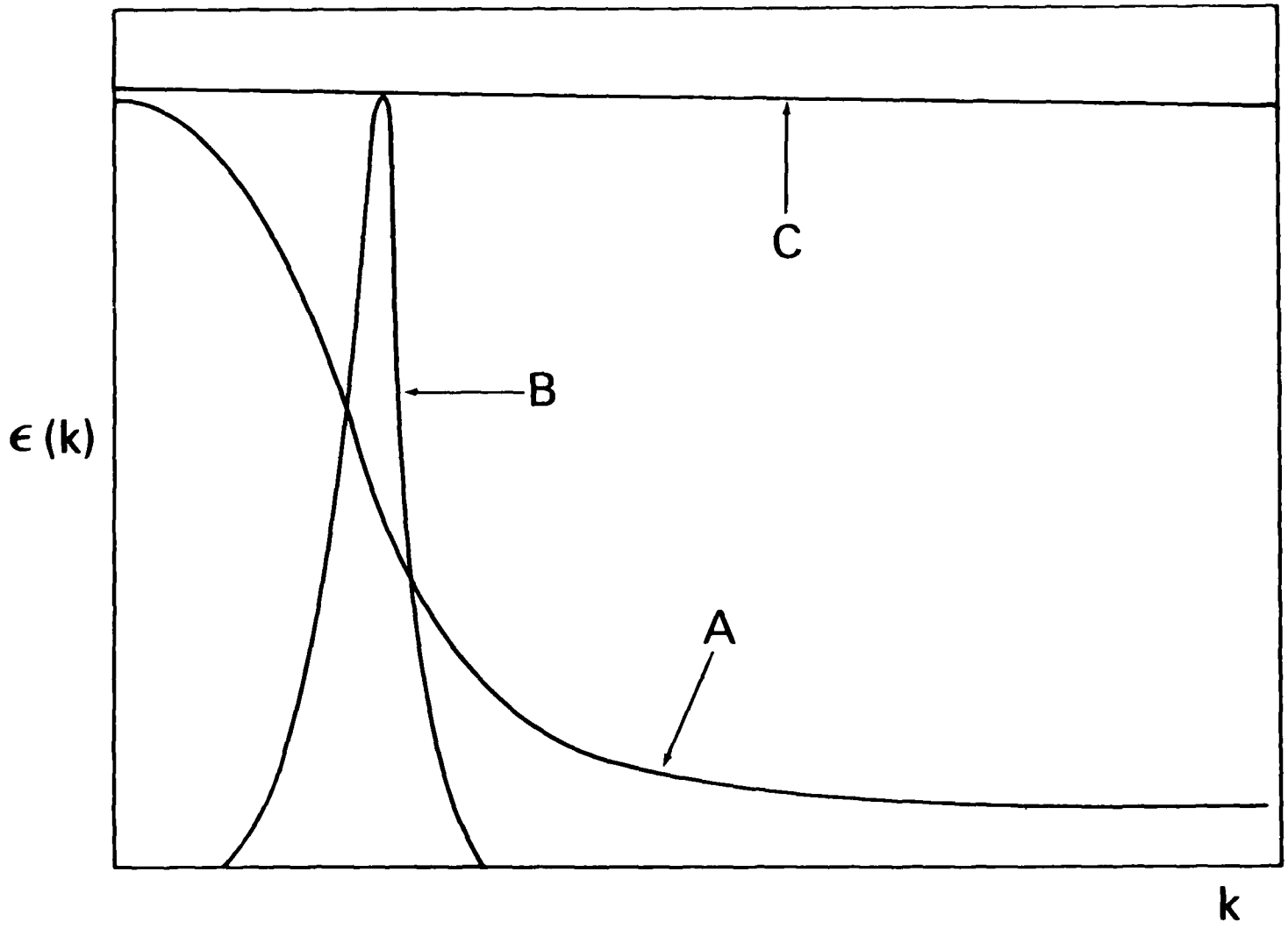

Fig. 1 — Schematic plot of $\epsilon(k_x,k_y)$, Curve A refers to previous simulations [McDonald et al., 1978; 1980; Keskinen et al., 1980] and has a Gaussian dependence on $k = (k_x^2 + k_y^2)^{1/2}$. Curve B represents a delta function in k_y while curve C is approximately flat in k.

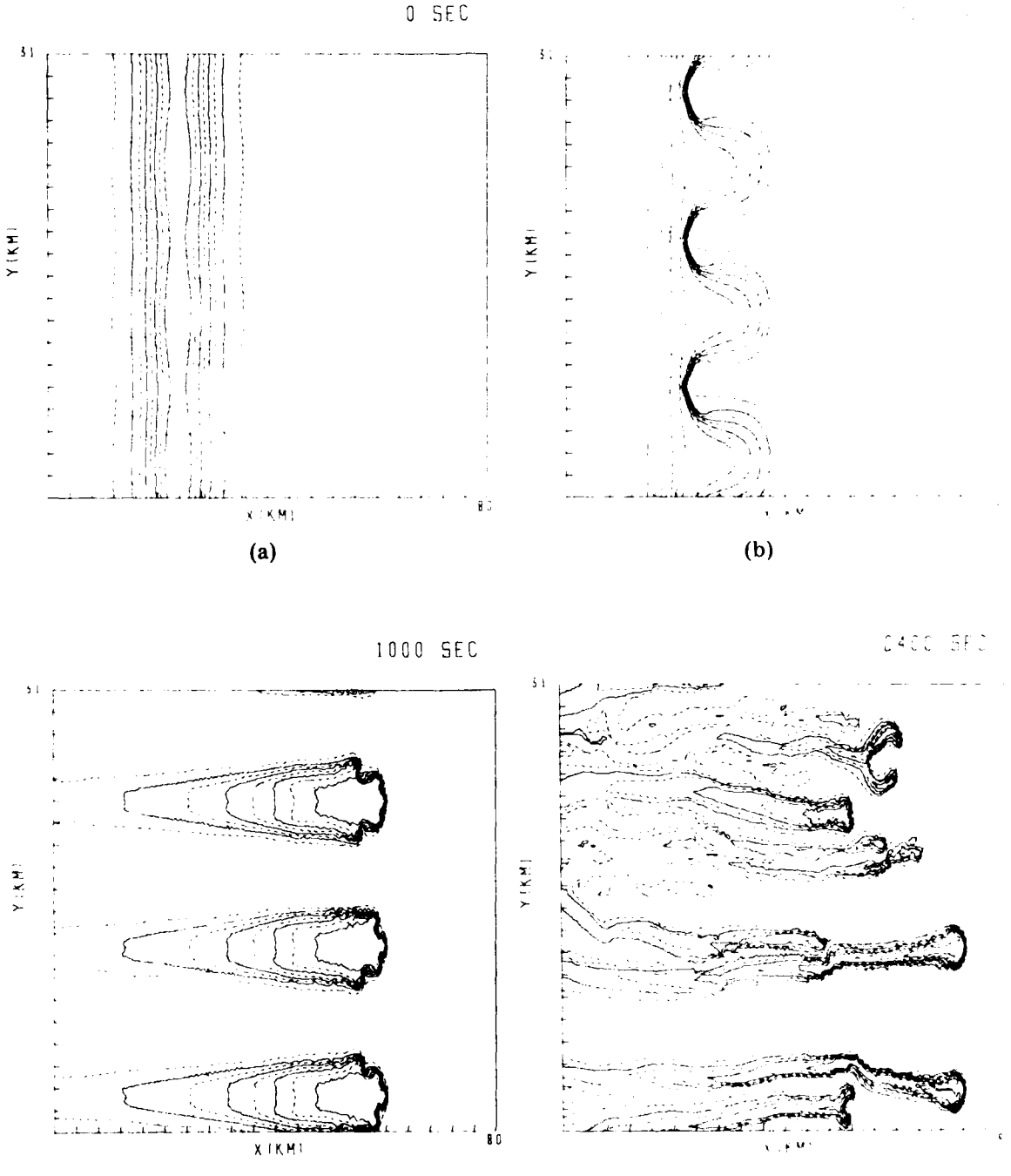

Fig. 2 — Real space isodensity contour plots of $\Sigma(x,y)/\Sigma_o$ for L = 6 km using 3% monochromatic initial conditions at (a) t = 0 sec, (b) t = 200 sec, (c) t = 1000 sec, and (d) t = 2400 sec. Eight contours are plotted in equal increments from 0.1 to 1 with every other contour represented by a dashed line. The x axis (y axis) denotes the $\underline{E}_o \times \underline{B}(\underline{E}_o)$ direction.

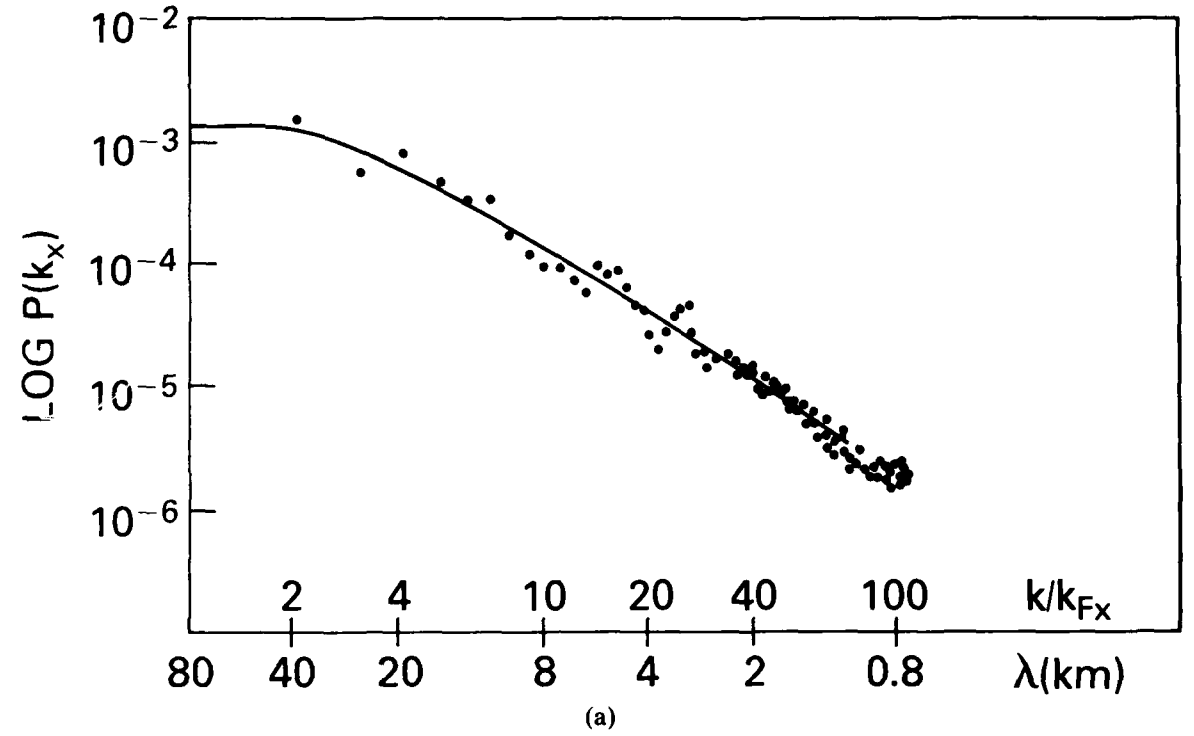

(a)

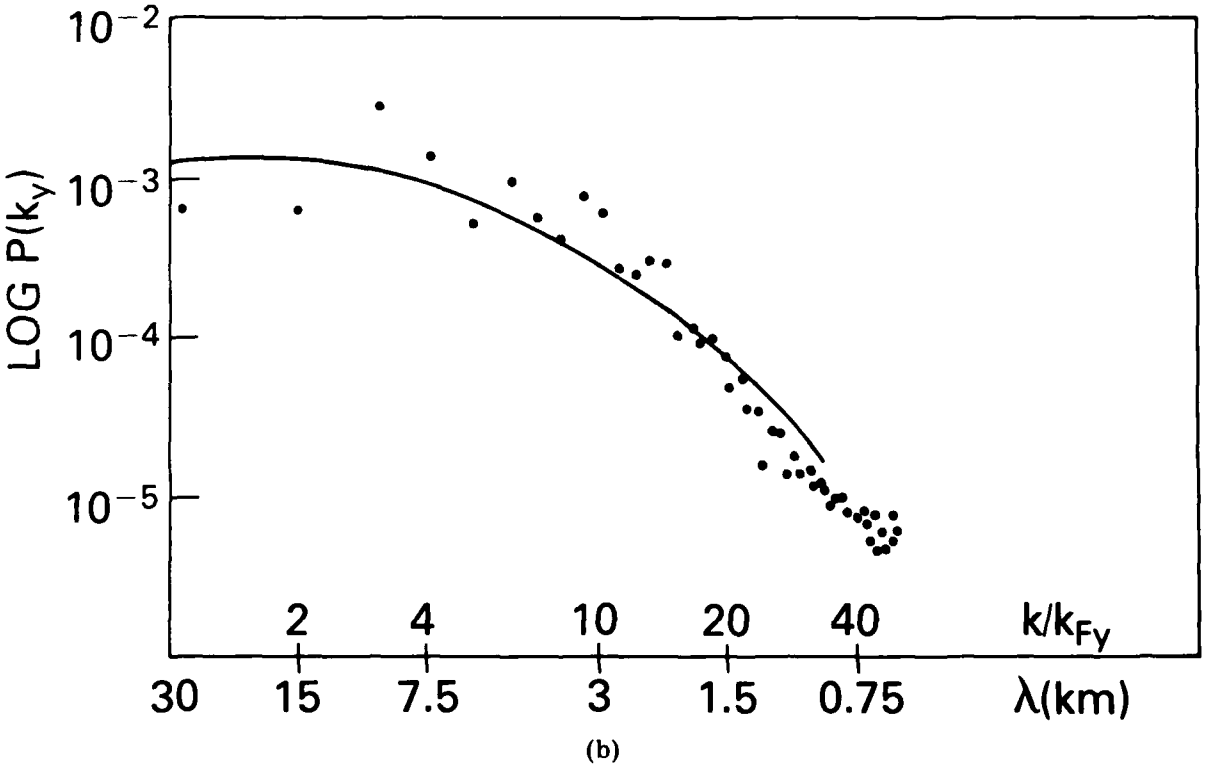

(b)

Fig. 3 — One dimensional (a) x power spectra $P(k_x)$ and (b) y power $P(k_y)$ at t = 2400 sec for L = 6 km using 3% monochromatic initial conditions. In (a) $k_{Fx} = 2\pi/80$ km^{-1} while in (b) $k_{Fy} = 2\pi/31$ km^{-1}. The dots represent the numerical simulation results; the solid curve is a least squares fit which yields in (a) $n_x = 1.9$ and in (b) $n_y = 1.7$.

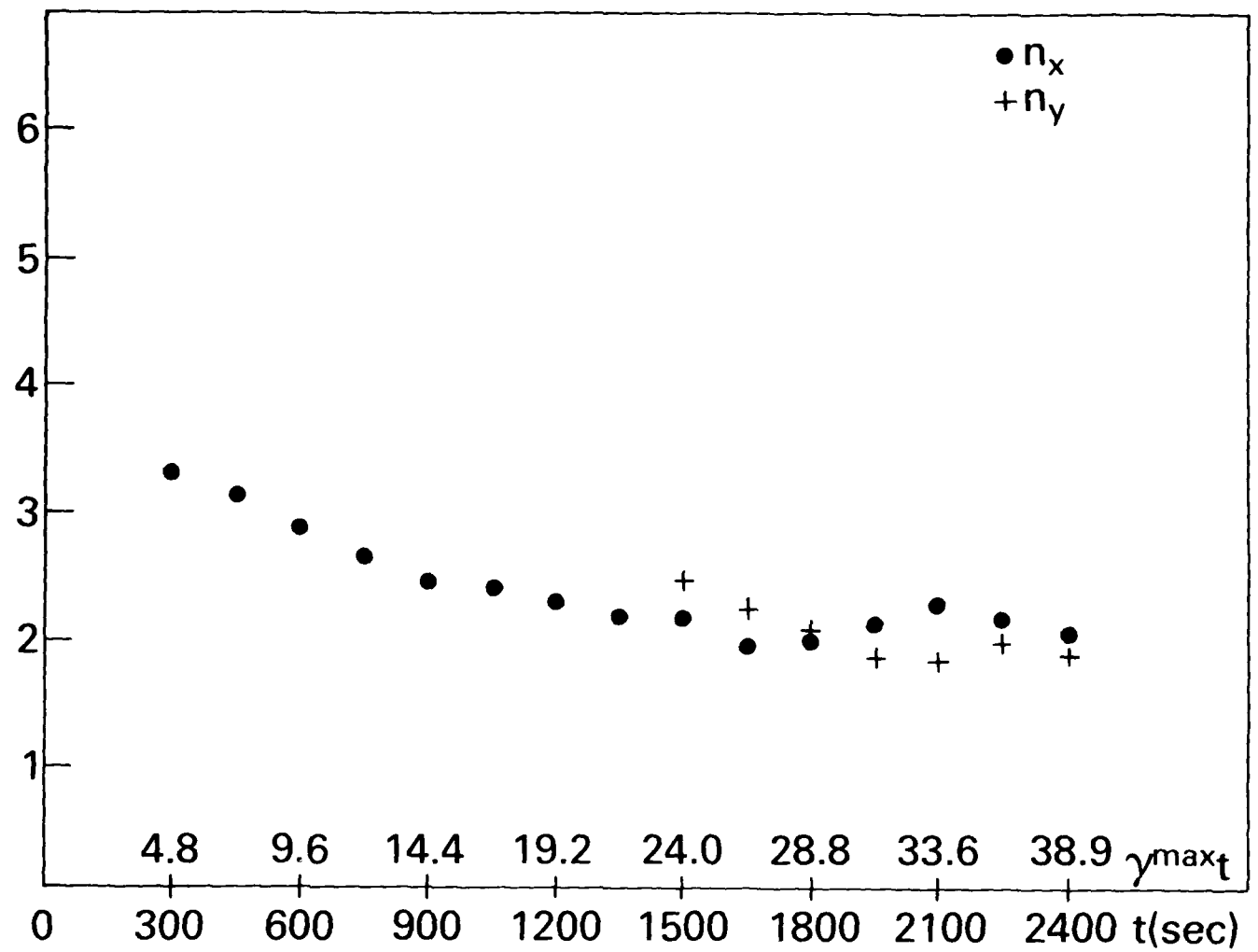

Fig. 4 — Time history of best fit spectral indices n_x and n_y for L = 6 km using the 3% monochromatic initial conditions. The spectral index n_y is not plotted before approximately 1500 sec since $P(k_y)$ is not a power law. γ^{max} is the maximum linear growth rate.

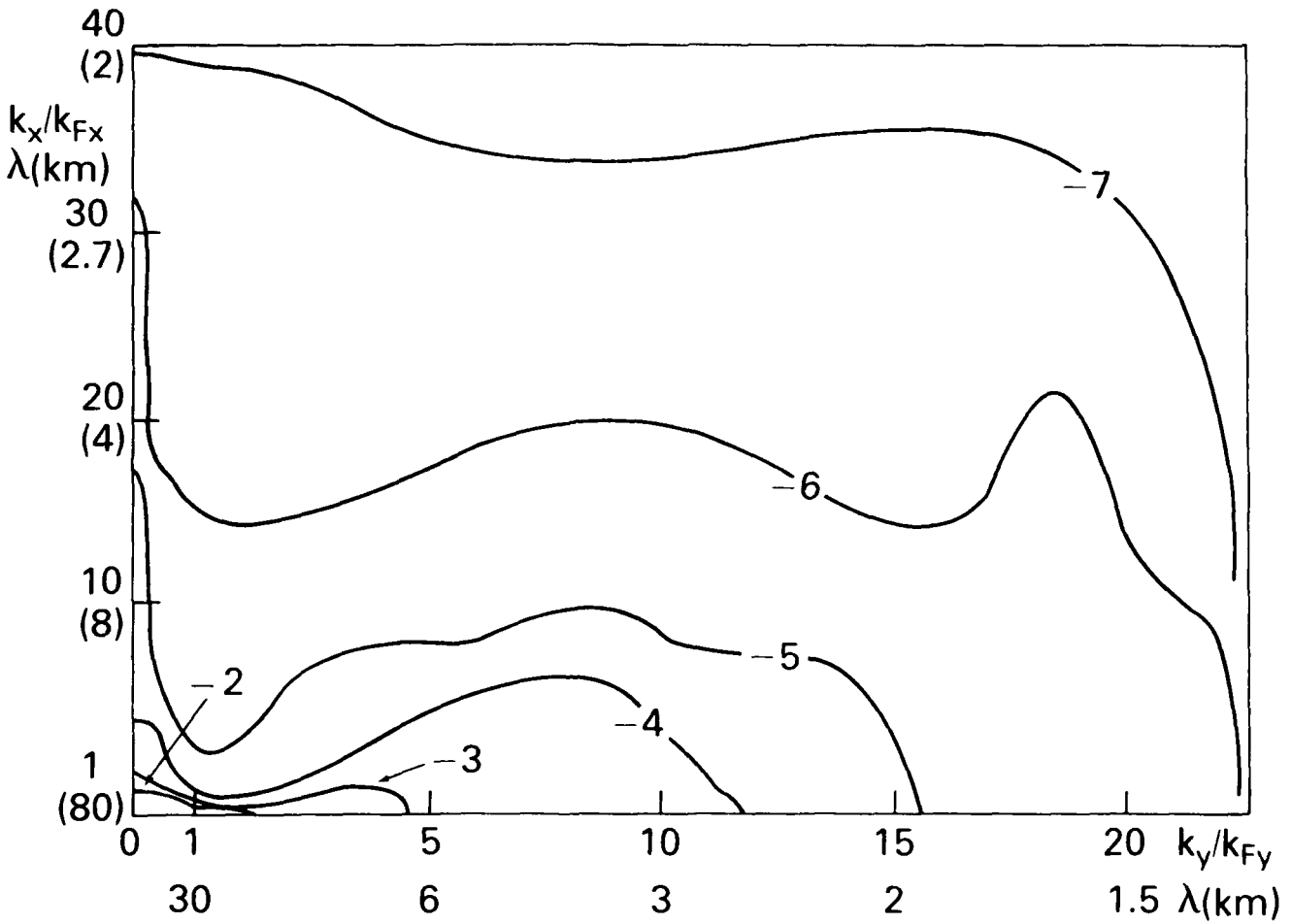

Fig. 5 — Contour plot of $\log_{10} |\delta\Sigma(k_x,k_y)/\Sigma_o|^2$ at t = 2400 sec for L = 6 km using the 3% monochromatic initial conditions. Six contours are plotted which correspond to decades of decreasing spectral power. The values of $k_{Fx} = 2\pi/80$ km^{-1} with $k_{Fy} = 2\pi/31$ km^{-1}.

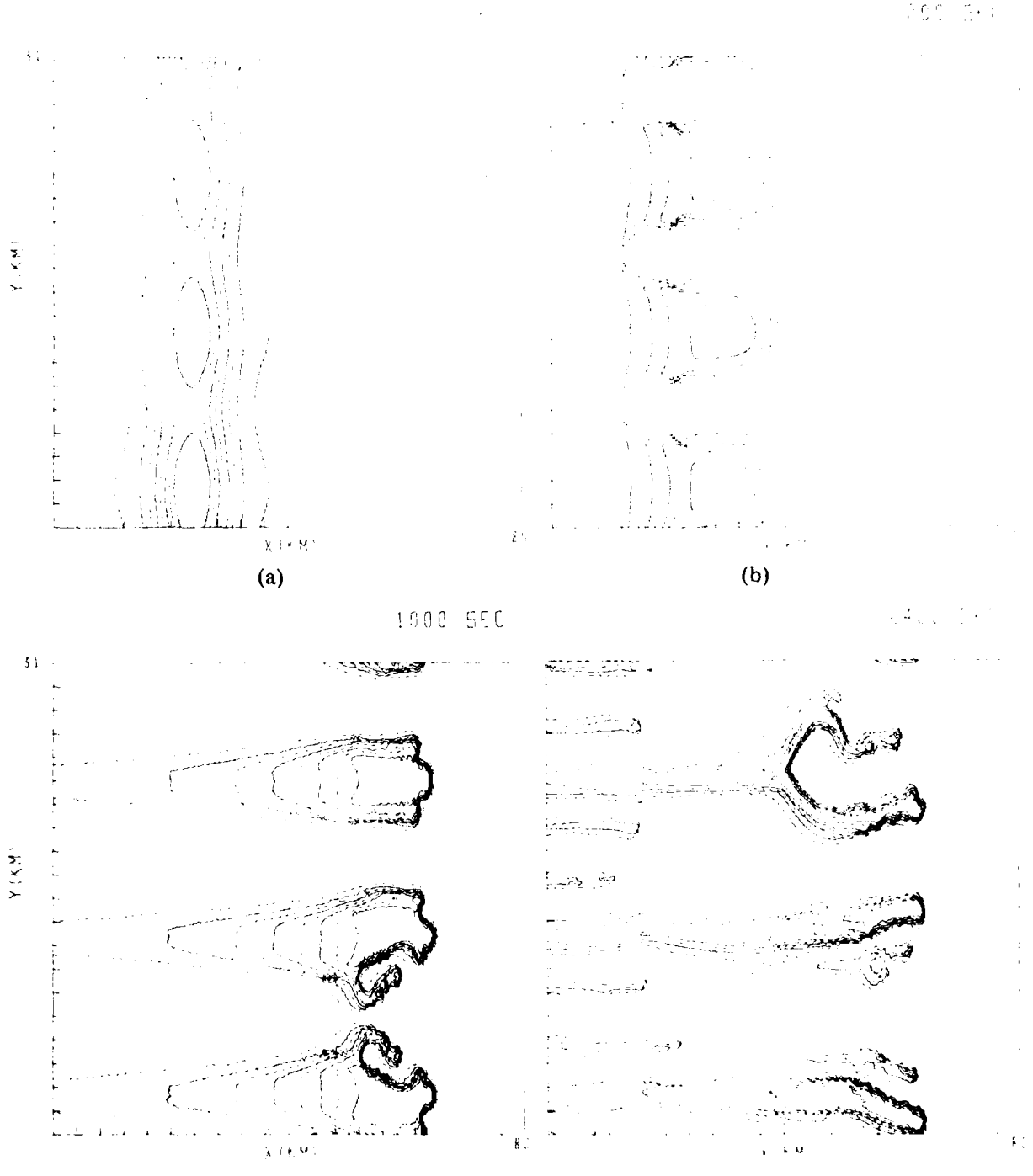

(a) (b)

(c) (d)

Fig. 6 — Real space isodensity contour plots of $\Sigma(x,y)/\Sigma_o$ for L = 6 km using the 15% monochromatic initial conditions at (a) t = 0 sec, (b) t = 200 sec, (c) t = 1000 sec, and (d) t = 2400 sec.

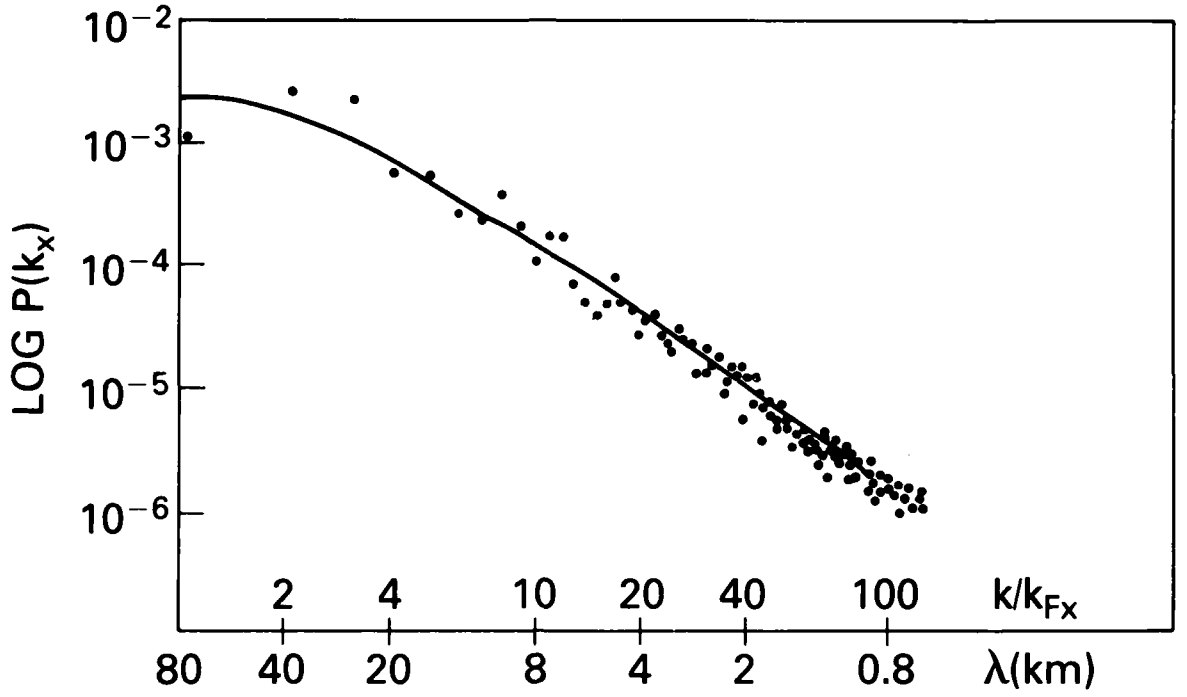

(a)

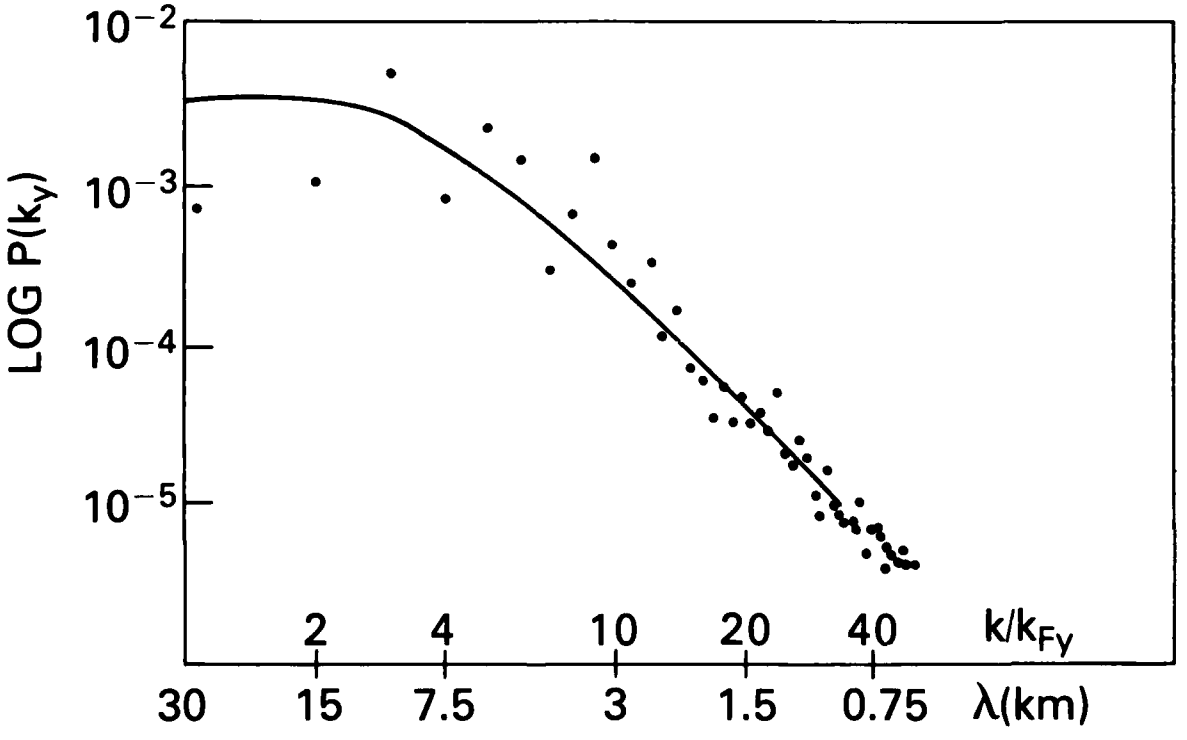

(b)

Fig. 7 — One dimensional (a) x power spectra $P(k_x)$ and (b) y power spectra $P(k_y)$ at t = 2400 sec for L = 6 km using the 15% monochromatic initial conditions with $n_x = 2.2$ and $n_y = 2.1$

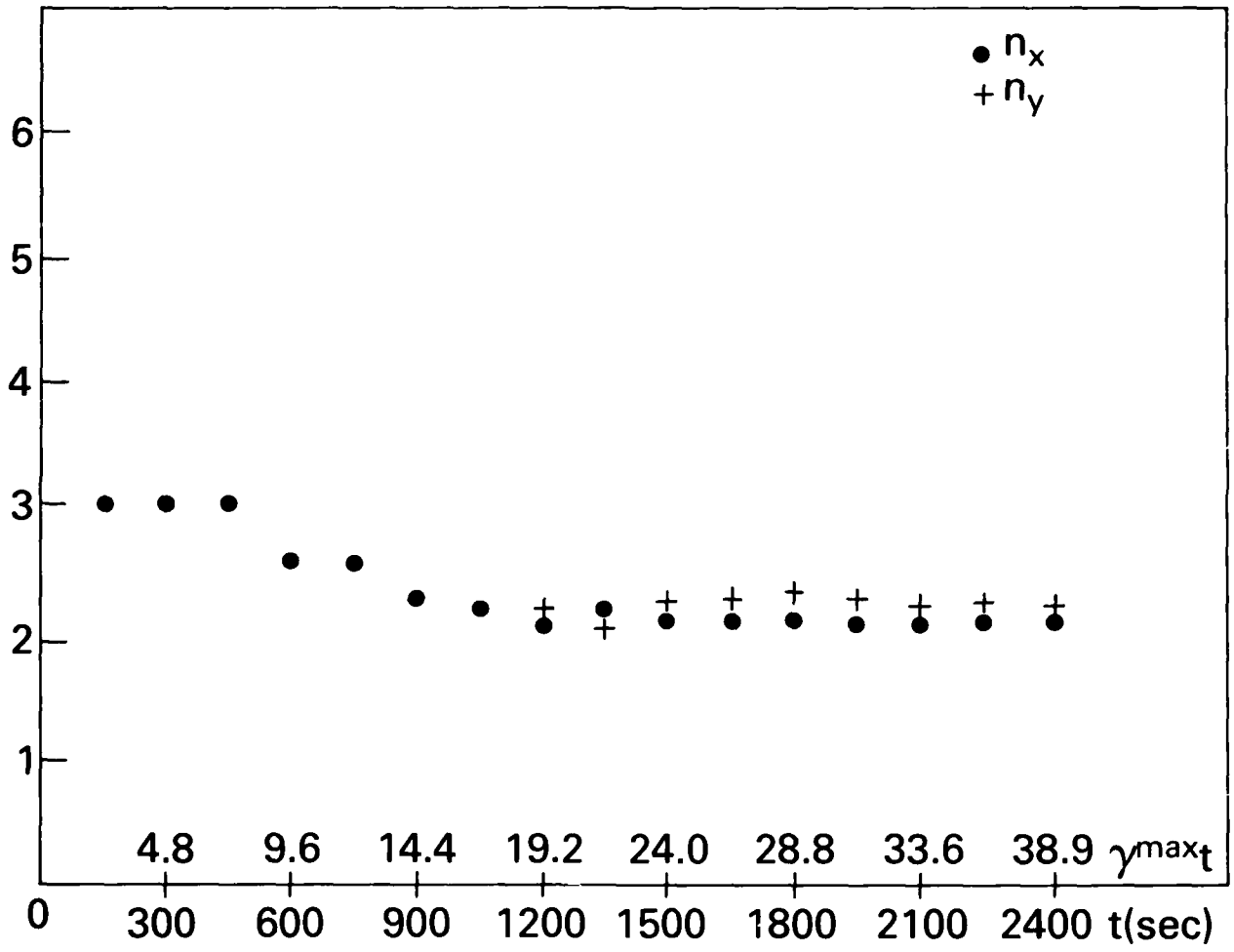

Fig. 8 — Time history of best fit spectral indices n_x and n_y for L = 6 km using the 15% monochromatic initial conditions. The spectral index n_y is not plotted before approximately 1200 sec since $P(k_y)$ is not a power law.

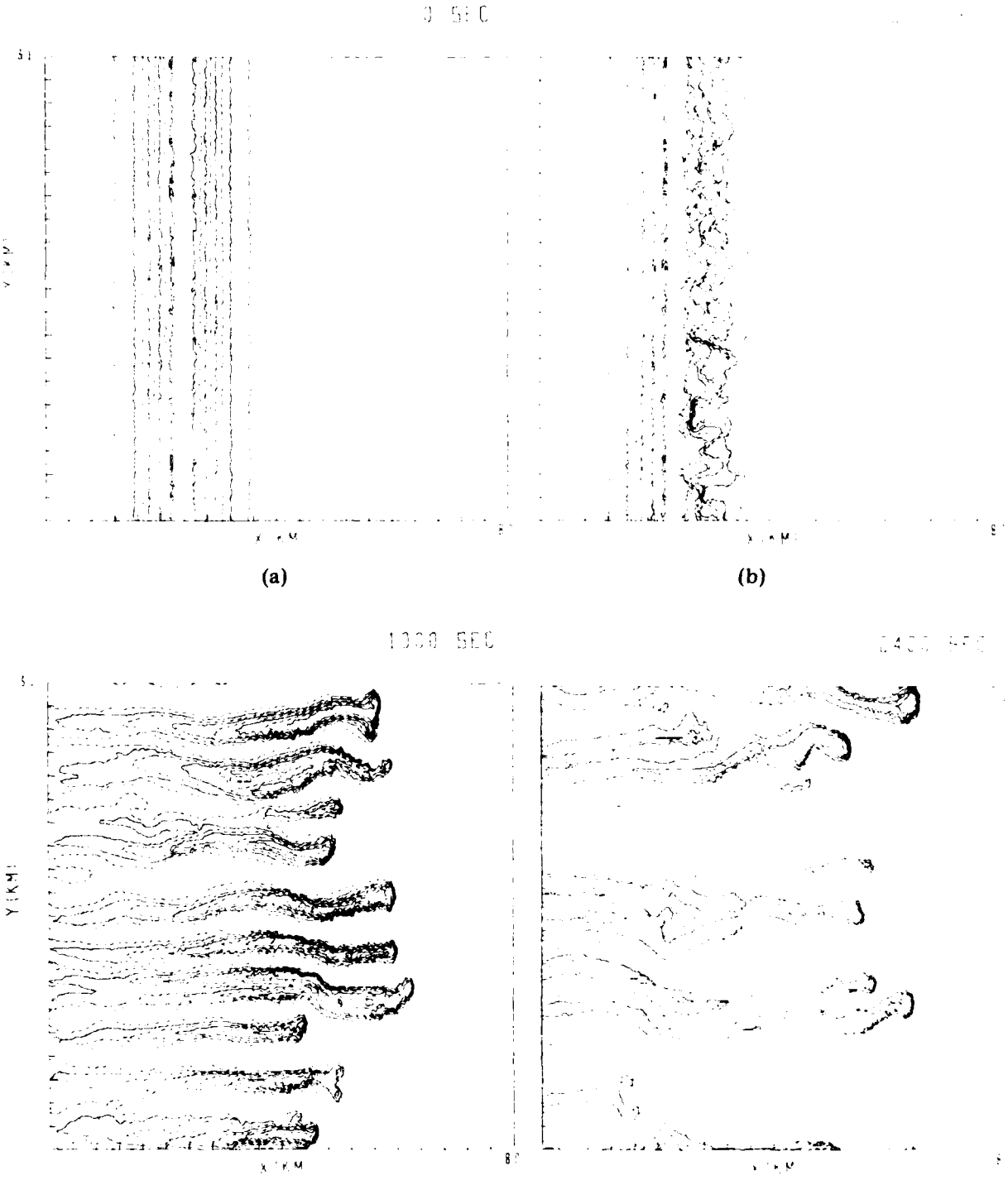

Fig. 9 — Real space isodensity contours plots of $\Sigma(x,y)/\Sigma_o$ for L = 6 km using the 3% random initial conditions at (a) t = 0 sec, (b) t = 200 sec, (d) t = 1000 sec, and (d) t = 2400 sec

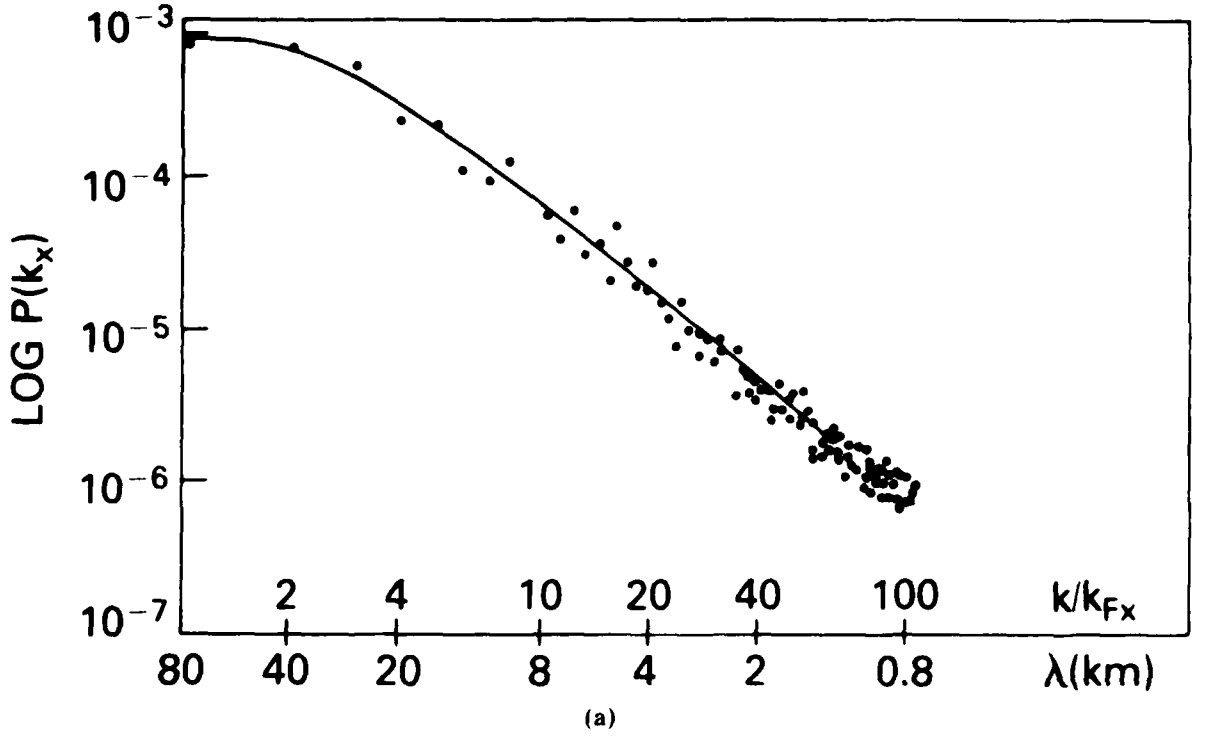

(a)

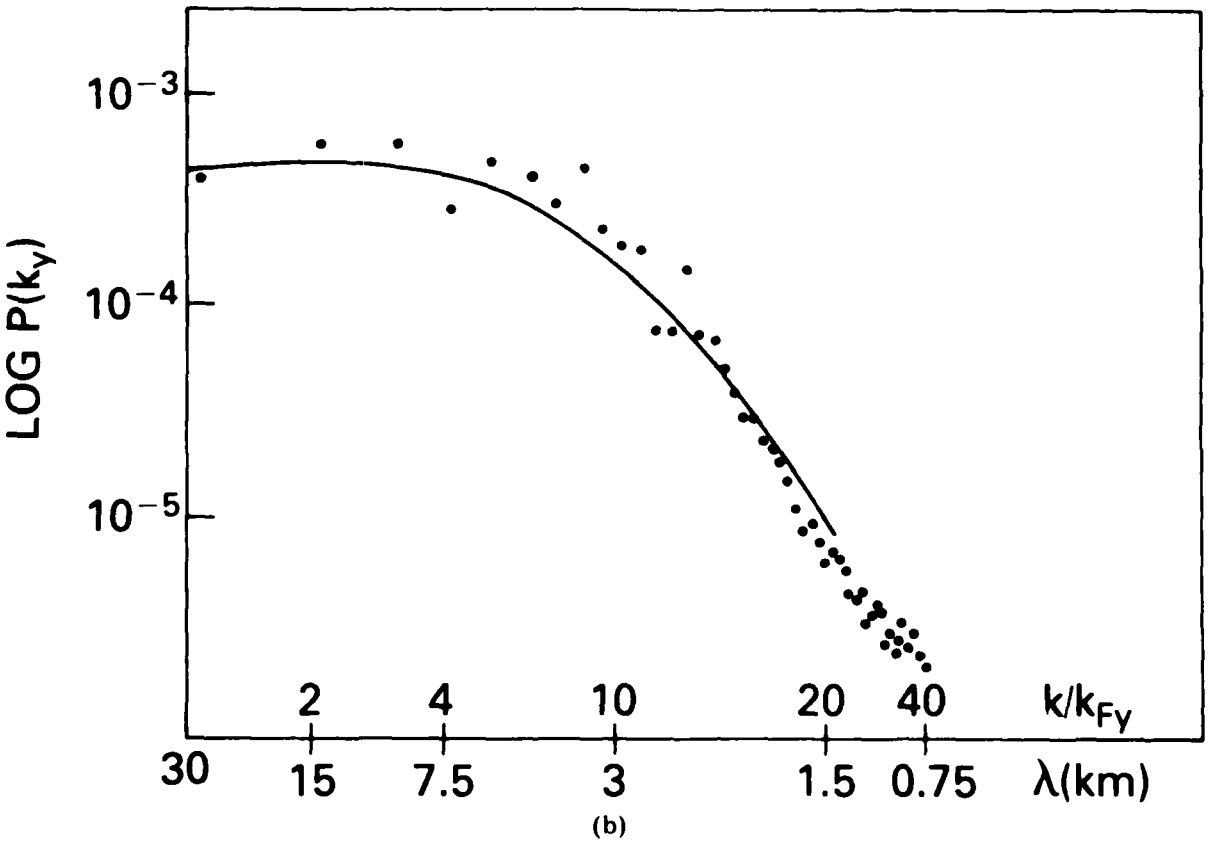

(b)

Fig. 10 — One dimensional (a) x power spectra $P(k_x)$ and (b) y power spectra $P(k_y)$ at t = 2400 sec for L = 6 km using the 3% random initial conditions with n_x = 2.0, $2\pi/k_{ox}$ = 32 km, and n_y = 2.4, $2\pi/k_{oy}$ = 3.8 km

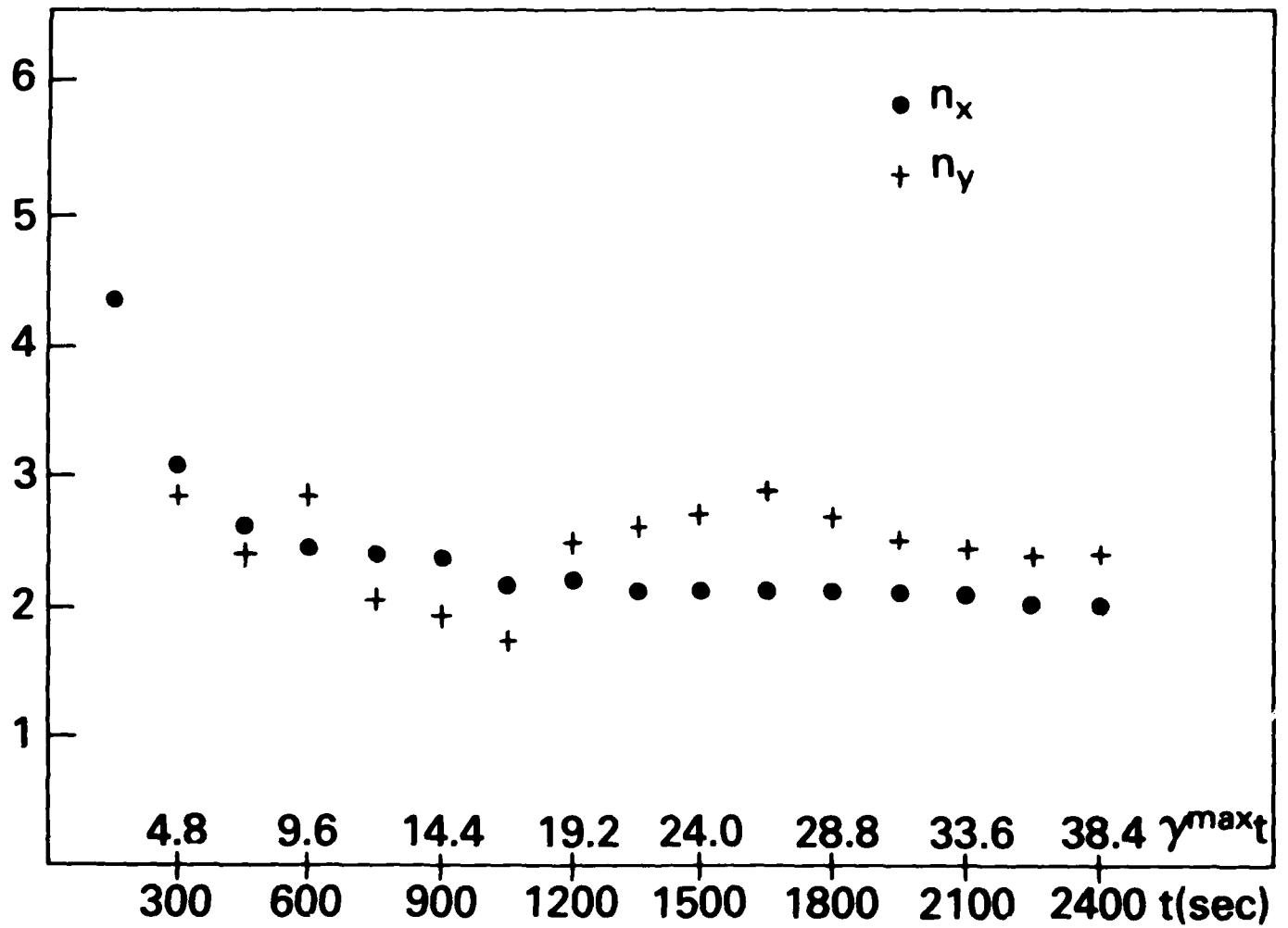

Fig. 11 — Time history of best fit spectral indices n_x and n_y for L = 6 km using the 3% random initial perturbations

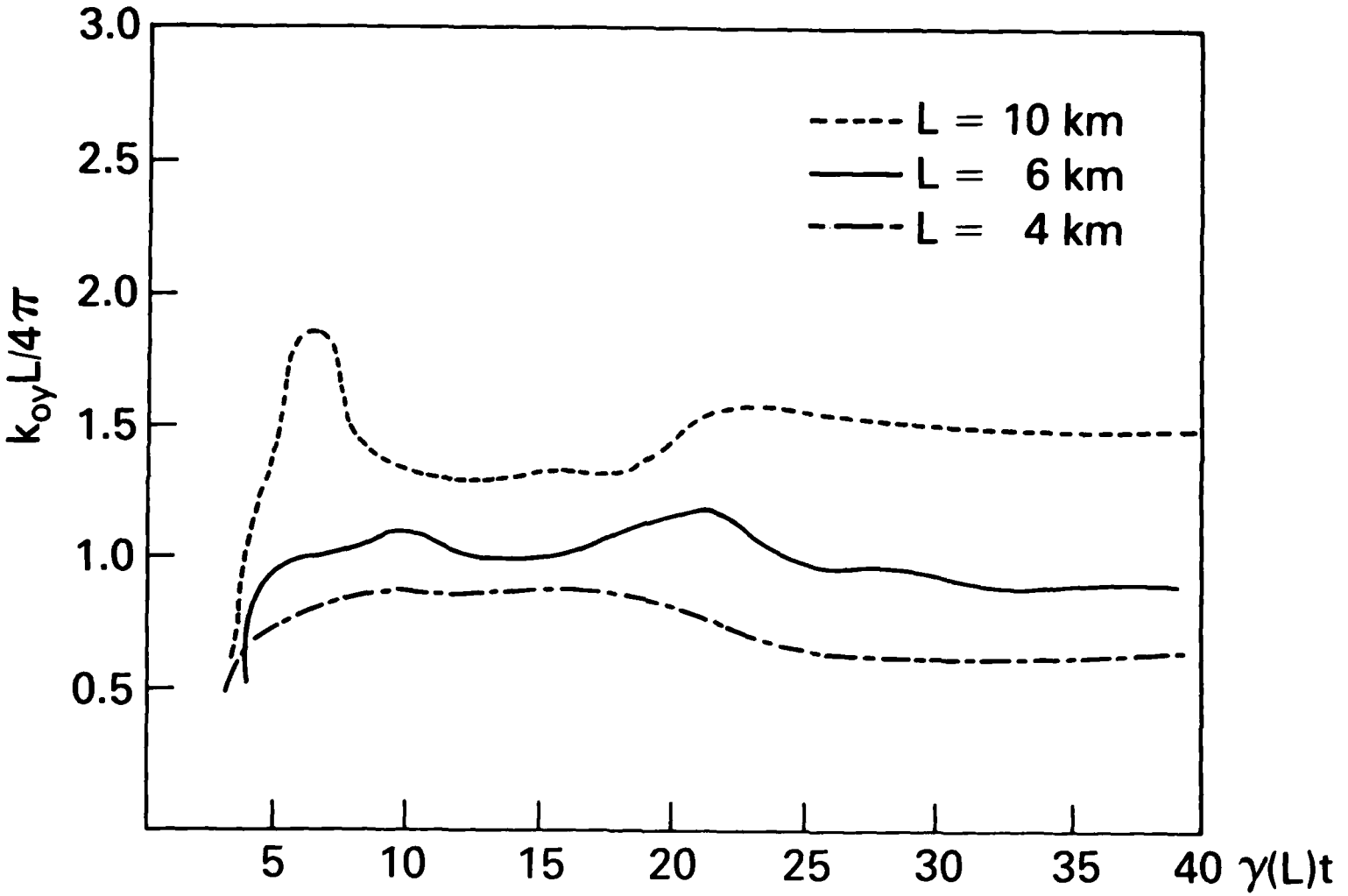

Fig. 12 — Time history of $k_{oy}L/4\pi$ for 4, 6, 10 km using the 3% random initial conditions. $\gamma(L)$ is maximum linear growth rate.

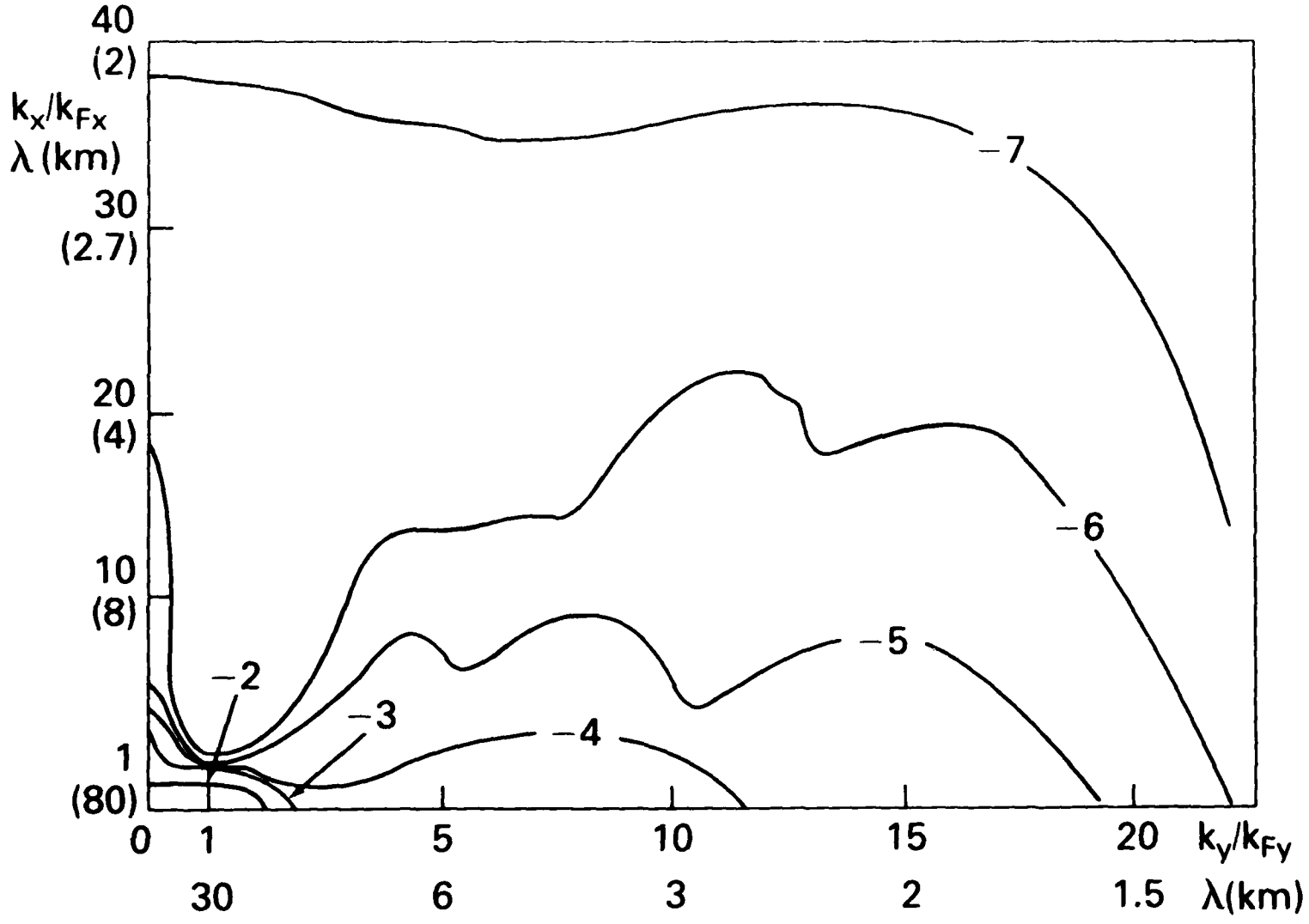

Fig. 13 — Contour plot of $\log_{10} |\delta\Sigma(k_x,k_y)/\Sigma_o|^2$ at t = 2400 sec for L = 6 km using the 3% random initial conditions

Fig. 14 — Real space isodensity contour plots of $\Sigma(x,y)/\Sigma_o$ for L = 6 km using the 15% random initial conditions at (a) t = 0 sec, (b) t = 200 sec, (c) t = 1000 sec, and (d) = 2400 sec

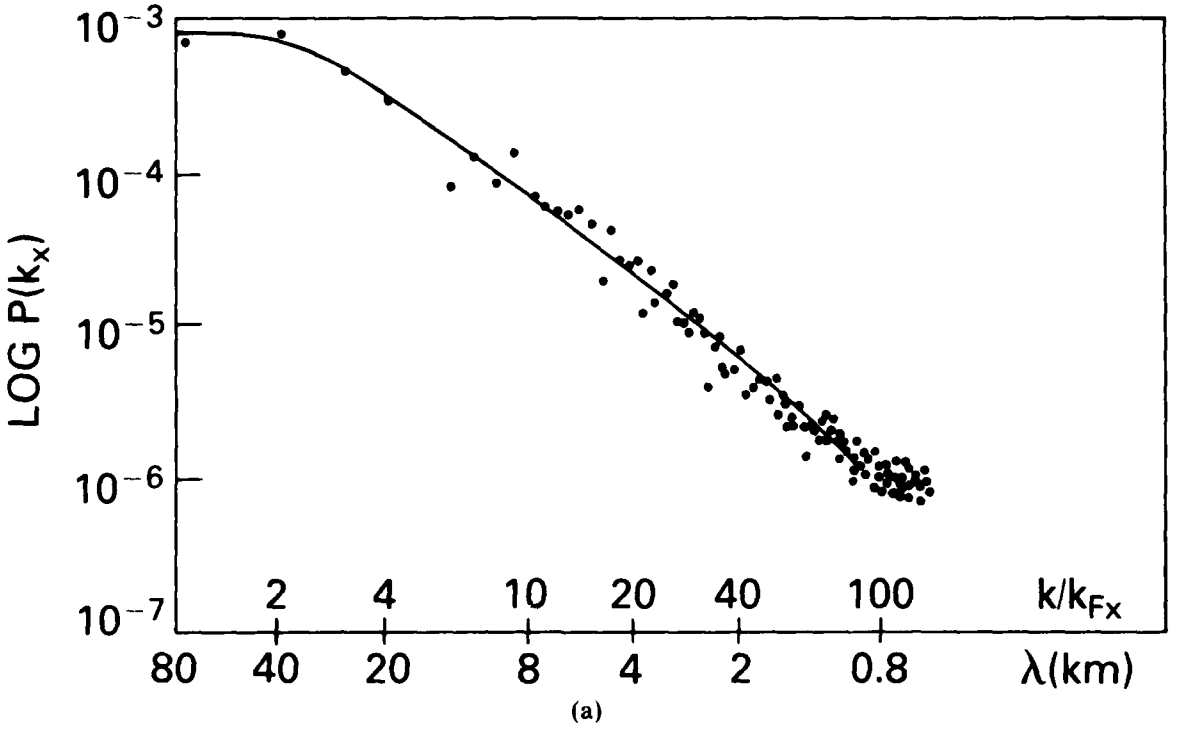

(a)

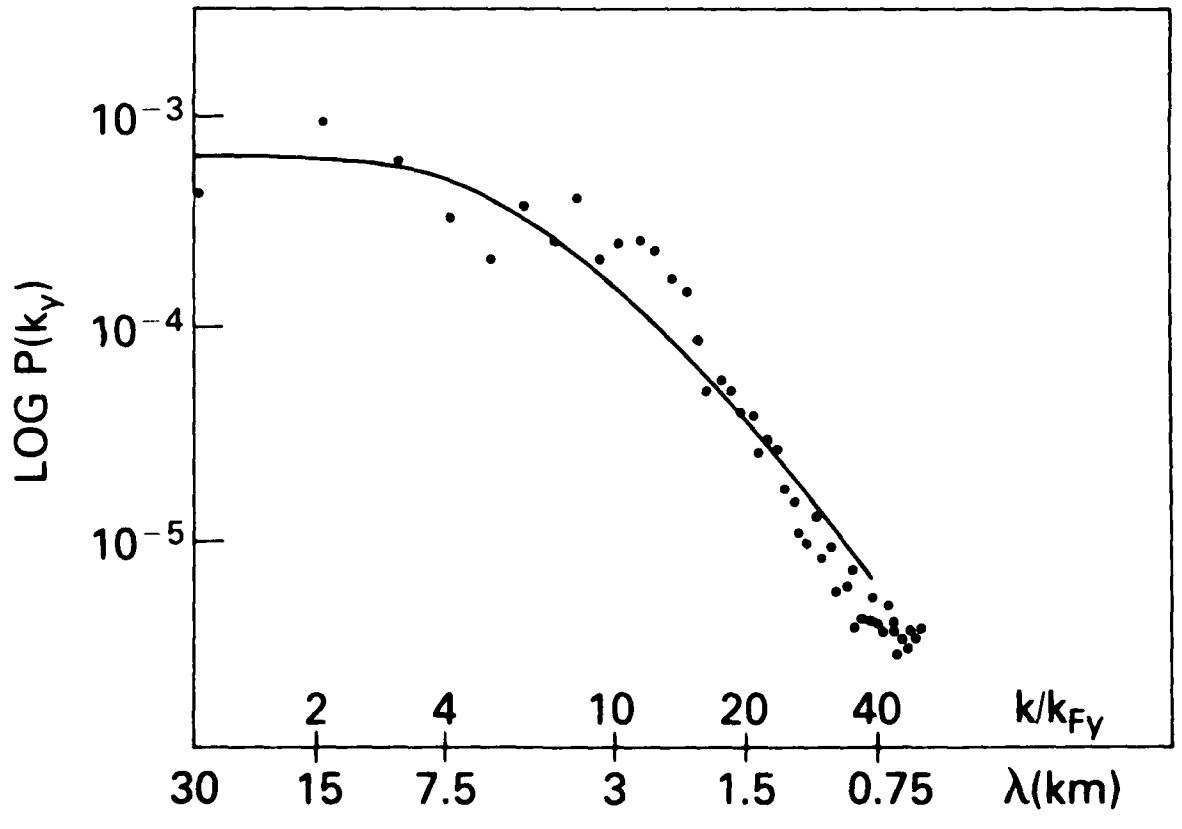

(b)

Fig. 15 — One dimensional (a) x power spectra $P(k_x)$ and (b) y power $P(k_y)$ at t = 2400 sec for L = 6 km using the 15% random initial conditions with $n_x = 2.0$, $2\pi/k_{ox} = 30$ km and $n_y = 2.3$, $2\pi/k_{oy} = 3.9$ km

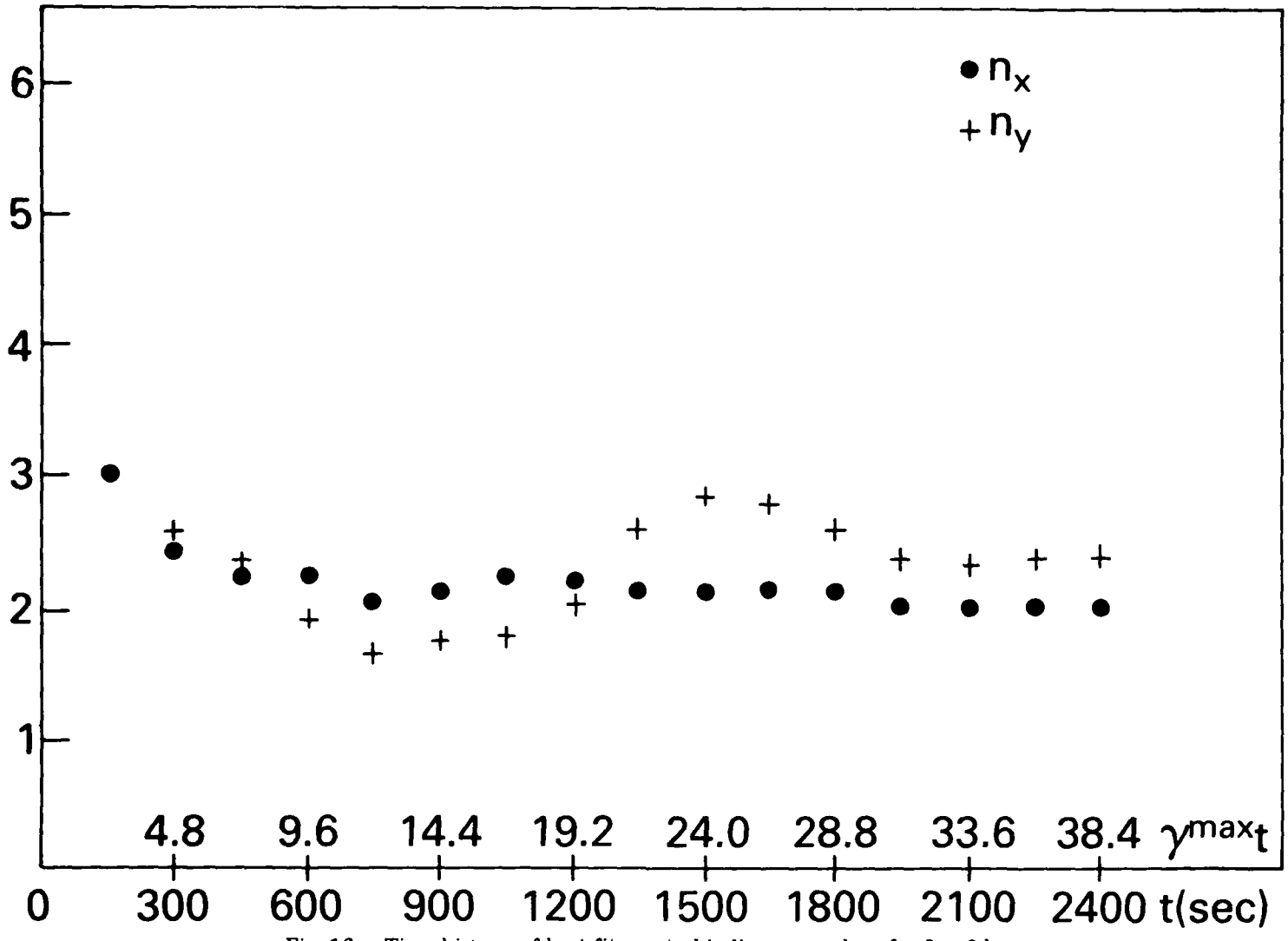

Fig. 16 — Time history of best fit spectral indices n_x and n_y for L = 6 km using the 15% random initial conditions

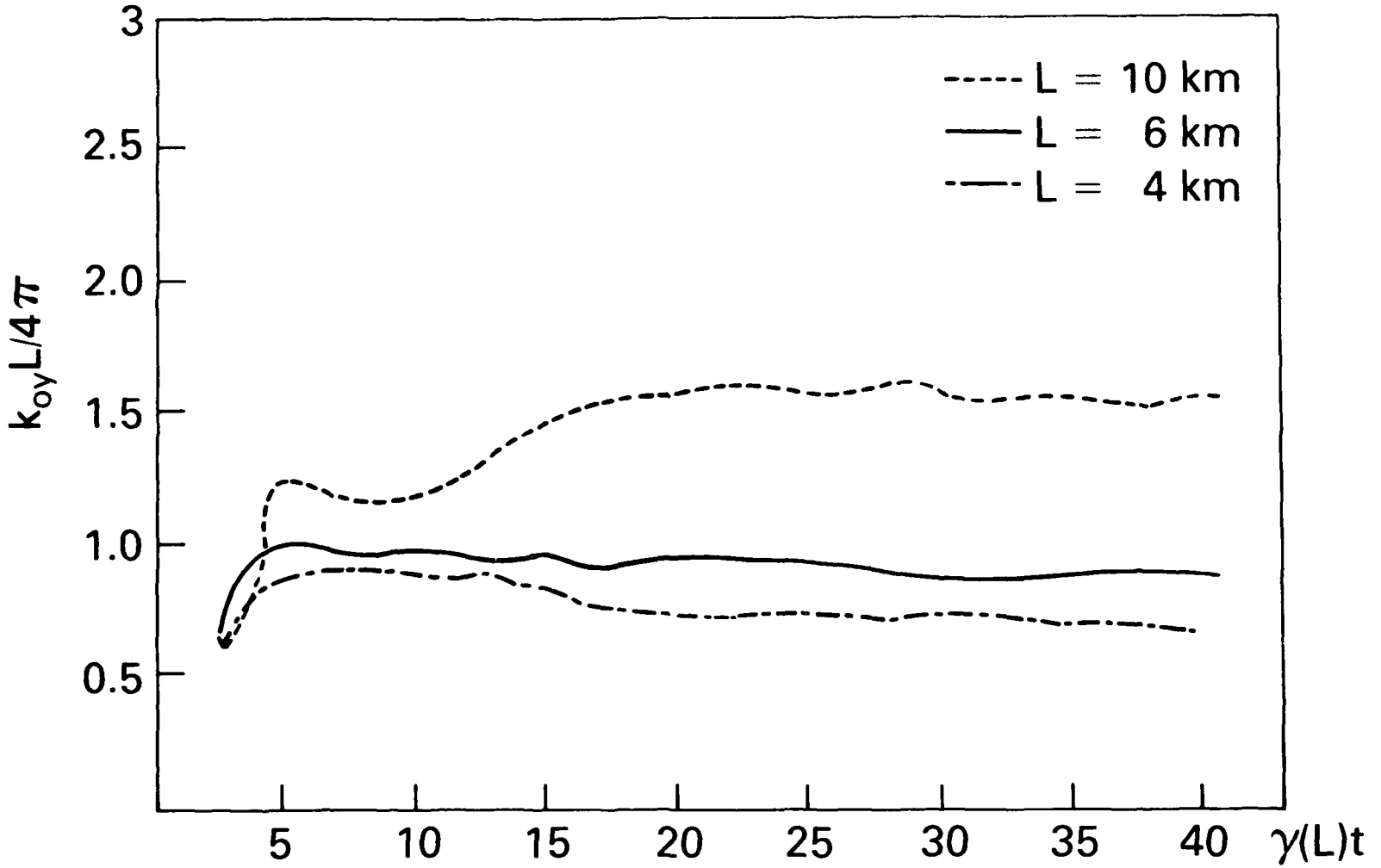

Fig. 17 — Time history for k_{oy} $L/4\pi$ for L = 4, 6, 10 km using the 15% random initial conditions. $\gamma(L)$ is maximum linear growth rate.

DISTRIBUTION LIST

DEPARTMENT OF DEFENSE

ASSISTANT SECRETARY OF DEFENSE
COMM, CMD, CONT & INTELL
WASHINGTON, D.C. 20301
01CY ATTN J. BABCOCK
01CY ATTN M. EPSTEIN

ASSISTANT TO THE SECRETARY OF DEFENSE
ATOMIC ENERGY
WASHINGTON, D.C. 20301
01CY ATTN EXECUTIVE ASSISTANT

DIRECTOR
COMMAND CONTROL TECHNICAL CENTER
PENTAGON RM BE 685
WASHINGTON, D.C. 20301
01CY ATTN C-650
01CY ATTN C-312 R. MASON

DIRECTOR
DEFENSE ADVANCED RSCH PROJ AGENCY
ARCHITECT BUILDING
1400 WILSON BLVD.
ARLINGTON, VA. 22209
01CY ATTN NUCLEAR MONITORING RESEARCH
01CY ATTN STRATEGIC TECH OFFICE

DEFENSE COMMUNICATION ENGINEER CENTER
1860 WIEHLE AVENUE
RESTON, VA. 22090
01CY ATTN CODE R820
01CY ATTN CODE R410 JAMES W. MCLEAN
01CY ATTN CODE R720 J. WORTHINGTON

DIRECTOR
DEFENSE COMMUNICATIONS AGENCY
WASHINGTON, D.C. 20305
(ADR CNWDI: ATTN CODE 240 FOR)
01CY ATTN CODE 1018

DEFENSE TECHNICAL INFORMATION CENTER
CAMERON STATION
ALEXANDRIA, VA. 22314
(12 COPIES IF OPEN PUBLICATION, OTHERWISE 2 COPIES)
12CY ATTN TC

DIRECTOR
DEFENSE INTELLIGENCE AGENCY
WASHINGTON, D.C. 20301
01CY ATTN DT-1B
01CY ATTN DB-4C E. O'FARRELL
01CY ATTN DIAAP A. WISE
01CY ATTN DIAST-5
01CY ATTN DT-1BZ R. MORTON
01CY ATTN HQ-TR J. STEWART
01CY ATTN W. WITTIG DC-7D

DIRECTOR
DEFENSE NUCLEAR AGENCY
WASHINGTON, D.C. 20305
01CY ATTN STVL
04CY ATTN TITL
01CY ATTN DDST
03CY ATTN RAAE

COMMANDER
FIELD COMMAND
DEFENSE NUCLEAR AGENCY
KIRTLAND AFB, NM 87115
01CY ATTN FCPR

DIRECTOR
INTERSERVICE NUCLEAR WEAPONS SCHOOL
KIRTLAND AFB, NM 87115
01CY ATTN DOCUMENT CONTROL

JOINT CHIEFS OF STAFF
WASHINGTON, D.C. 20301
01CY ATTN J-3 WWMCCS EVALUATION OFFICE

DIRECTOR
JOINT STRAT TGT PLANNING STAFF
OFFUTT AFB
OMAHA, NB 68113
01CY ATTN JLTW-2
01CY ATTN JPST G. GOETZ

CHIEF
LIVERMORE DIVISION FLD COMMAND DNA
DEPARTMENT OF DEFENSE
LAWRENCE LIVERMORE LABORATORY
P. O. BOX 808
LIVERMORE, CA 94550
01CY ATTN FCPRL

DIRECTOR
NATIONAL SECURITY AGENCY
DEPARTMENT OF DEFENSE
FT. GEORGE G. MEADE, MD 20755
01CY ATTN JOHN SKILLMAN R52
01CY ATTN FRANK LEONARD
01CY ATTN W14 PAT CLARK
01CY ATTN OLIVER H. BARTLETT W32
01CY ATTN R5

COMMANDANT
NATO SCHOOL (SHAPE)
APO NEW YORK 09172
01CY ATTN U.S. DOCUMENTS OFFICER

UNDER SECY OF DEF FOR RSCH & ENGRG
DEPARTMENT OF DEFENSE
WASHINGTON, D.C. 20301
01CY ATTN STRATEGIC & SPACE SYSTEMS (OS)

WWMCCS SYSTEM ENGINEERING ORG
WASHINGTON, D.C. 20305
01CY ATTN R. CRAWFORD

COMMANDER/DIRECTOR
ATMOSPHERIC SCIENCES LABORATORY
U.S. ARMY ELECTRONICS COMMAND
WHITE SANDS MISSILE RANGE, NM 88002
01CY ATTN DELAS-EO F. NILES

DIRECTOR
BMD ADVANCED TECH CTR
HUNTSVILLE OFFICE
P. O. BOX 1500
HUNTSVILLE, AL 35807
01CY ATTN ATC-T MELVIN T. CAPPS
01CY ATTN ATC-O W. DAVIES
01CY ATTN ATC-R DON RUSS

PROGRAM MANAGER
BMD PROGRAM OFFICE
5001 EISENHOWER AVENUE
ALEXANDRIA, VA 22333
01CY ATTN DACS-BMT J. SHEA

CHIEF C-E SERVICES DIVISION
U.S. ARMY COMMUNICATIONS CMD
PENTAGON RM 1B269
WASHINGTON, D.C. 20310
01CY ATTN C-E-SERVICES DIVISION

COMMANDER
FRADCOM TECHNICAL SUPPORT ACTIVITY
DEPARTMENT OF THE ARMY
FORT MONMOUTH, N.J. 07703
01CY ATTN DRSEL-NL-RD H. BENNET
01CY ATTN DRSEL-PL-ENV H. BOMKE
01CY ATTN J. E. QUIGLEY

COMMANDER
HARRY DIAMOND LABORATORIES
DEPARTMENT OF THE ARMY
2800 POWDER MILL ROAD
ADELPHI, MD 20783
(CNWDI-INNER ENVELOPE: ATTN: DELHD-RBH)
01CY ATTN DELHD-TI M. WEINER
01CY ATTN DELHD-RB R. WILLIAMS
01CY ATTN DELHD-NP F. WIMENITZ
01CY ATTN DELHD-NP C. MOAZED

COMMANDER
U.S. ARMY COMM-ELEC ENGRG INSTAL AGY
FT. HUACHUCA, AZ 85613

01CY ATTN CCC-EMEO GEORGE LANE

COMMANDER
U.S. ARMY FOREIGN SCIENCE & TECH CTR
220 7TH STREET, NE
CHARLOTTESVILLE, VA 22901
01CY ATTN DRXST-SD
01CY ATTN R. JONES

COMMANDER
U.S. ARMY MATERIEL DEV & READINESS CMD
5001 EISENHOWER AVENUE
ALEXANDRIA, VA 22333
01CY ATTN DRCLDC J. A. BENDER

COMMANDER
U.S. ARMY NUCLEAR AND CHEMICAL AGENCY
7500 BACKLICK ROAD
BLDG 2073
SPRINGFIELD, VA 22150
01CY ATTN LIBRARY

DIRECTOR
U.S. ARMY BALLISTIC RESEARCH LABS
ABERDEEN PROVING GROUND, MD 21005
01CY ATTN TECH LIB EDWARD BAICY

COMMANDER
U.S. ARMY SATCOM AGENCY
FT. MONMOUTH, NJ 07703
01CY ATTN DOCUMENT CONTROL

COMMANDER
U.S. ARMY MISSILE INTELLIGENCE AGENCY
REDSTONE ARSENAL, AL 35809
01CY ATTN JIM GAMBLE

DIRECTOR
U.S. ARMY TRADOC SYSTEMS ANALYSIS ACTIVITY
WHITE SANDS MISSILE RANGE, NM 88002
01CY ATTN ATAA-SA
01CY ATTN TCC/F. PAYAN JR.
01CY ATTN ATAA-TAC LTC J. HESSE

COMMANDER
NAVAL ELECTRONIC SYSTEMS COMMAND
WASHINGTON, D.C. 20360
01CY ATTN NAVALEX 034 T. HUGHES
01CY ATTN PME 117
01CY ATTN PME 117-T
01CY ATTN CODE 5011

COMMANDING OFFICER
NAVAL INTELLIGENCE SUPPORT CTR
4301 SUITLAND ROAD, BLDG. 5
WASHINGTON, D.C. 20390
01CY ATTN MR. DUBBIN STIC 12
01CY ATTN NISC-50
01CY ATTN CODE 5404 J. GALET

COMMANDER
NAVAL OCEAN SYSTEMS CENTER
SAN DIEGO, CA 92152
03CY ATTN CODE 532 W. MOLER
01CY ATTN CODE 0230 C. BAGGETT
01CY ATTN CODE 81 R. EASTMAN

DIRECTOR
NAVAL RESEARCH LABORATORY
WASHINGTON, D.C. 20375
01CY ATTN CODE 4700 T. P. COFFEY (25 CYS IF UN, 1 CY IF CLASS)
01CY ATTN CODE 4701 JACK D. BROWN
01CY ATTN CODE 4780 BRANCH HEAD (150 CYS IF UN, 1 CY IF CLASS)
01CY ATTN CODE 7500 HQ COMM DIR BRUCE WALD
01CY ATTN CODE 7550 J. DAVIS
01CY ATTN CODE 7580
01CY ATTN CODE 7551
01CY ATTN CODE 7555
01CY ATTN CODE 4730 E. MCLEAN

COMMANDER
NAVAL SEA SYSTEMS COMMAND
WASHINGTON, D.C. 20362
01CY ATTN CAPT R. PITKIN

COMMANDER
NAVAL SPACE SURVEILLANCE SYSTEM
DAHLGREN, VA 22448
01CY ATTN CAPT J. H. BURTON

OFFICER-IN-CHARGE
NAVAL SURFACE WEAPONS CENTER
WHITE OAK, SILVER SPRING, MD 20910
01CY ATTN CODE F31

DIRECTOR
STRATEGIC SYSTEMS PROJECT OFFICE
DEPARTMENT OF THE NAVY
WASHINGTON, D.C. 20376
01CY ATTN NSP-2141
01CY ATTN NSSP-2722 FRED WIMBERLY

NAVAL SPACE SYSTEM ACTIVITY
P. O. BOX 92960
WORLDWAY POSTAL CENTER
LOS ANGELES, CALIF. 90009
01CY ATTN A. B. HAZZARD

COMMANDER
NAVAL SURFACE WEAPONS CENTER
DAHLGREN LABORATORY
DAHLGREN, VA 22448
01CY ATTN CODE DF-14 R. BUTLER

COMMANDING OFFICER
NAVY SPACE SYSTEMS ACTIVITY
P.O. BOX 92960
WORLDWAY POSTAL CENTER
LOS ANGELES, CA. 90009
01CY ATTN CODE 52

OFFICE OF NAVAL RESEARCH
ARLINGTON, VA 22217
01CY ATTN CODE 465
01CY ATTN CODE 461
01CY ATTN CODE 402
01CY ATTN CODE 420
01CY ATTN CODE 421

COMMANDER
AEROSPACE DEFENSE COMMAND/DC
DEPARTMENT OF THE AIR FORCE
ENT AFB, CO 80912
01CY ATTN DC MR. LONG

COMMANDER
AEROSPACE DEFENSE COMMAND/XPD
DEPARTMENT OF THE AIR FORCE
ENT AFB, CO 80912
01CY ATTN XPDQQ
01CY ATTN XP

AIR FORCE GEOPHYSICS LABORATORY
HANSCOM AFB, MA 01731
01CY ATTN OPR HAROLD GARDNER
01CY ATTN OPR-1 JAMES C. ULWICK
01CY ATTN LKB KENNETH S. W. CHAMPION
01CY ATTN OPR ALVA T. STAIR
01CY ATTN PHP JULES AARONS
01CY ATTN PHD JURGEN BUCHAU
01CY ATTN PHD JOHN P. MULLEN

AF WEAPONS LABORATORY
KIRTLAND AFB, NM 87117
01CY ATTN SUL
01CY ATTN CA ARTHUR H. GUENTHER
01CY ATTN DYC CAPT J. BARRY
01CY ATTN DYC JOHN M. KAMM
01CY ATTN DYT CAPT MARK A. FRY
01CY ATTN DES MAJ GARY GANONG
01CY ATTN DYC J. JANNI

AFTAC
PATRICK AFB, FL 32925
01CY ATTN TF/MAJ WILEY
01CY ATTN TN

AIR FORCE Wright Aeronautical Laboratories
WRIGHT-PATTERSON AFB, OH 45433
01CY ATTN AAD WADE HUNT
01CY ATTN AAD ALLEN JOHNSON

DEPUTY CHIEF OF STAFF
RESEARCH, DEVELOPMENT, & ACQ
DEPARTMENT OF THE AIR FORCE
WASHINGTON, D.C. 20330
01CY ATTN AFRDQ

HEADQUARTERS
ELECTRONIC SYSTEMS DIVISION/XR
DEPARTMENT OF THE AIR FORCE
HANSCOM AFB, MA 01731
01CY ATTN XR J. DEAS

HEADQUARTERS
ELECTRONIC SYSTEMS DIVISION/YSEA
DEPARTMENT OF THE AIR FORCE
HANSCOM AFB, MA 01731
01CY ATTN YSEA

HEADQUARTERS
ELECTRONIC SYSTEMS DIVISION/DC
DEPARTMENT OF THE AIR FORCE
HANSCOM AFB, MA 01731
01CY ATTN DCKC MAJ J.C. CLARK

COMMANDER
FOREIGN TECHNOLOGY DIVISION, AFSC
WRIGHT-PATTERSON AFB, OH 45433
01CY ATTN NICD LIBRARY
01CY ATTN ETDP B. BALLARD

COMMANDER
ROME AIR DEVELOPMENT CENTER, AFSC
GRIFFISS AFB, NY 13441
01CY ATTN DOC LIBRARY/TSLD
01CY ATTN OCSE V. COYNE

SAMSO/SZ
POST OFFICE BOX 92960
WORLDWAY POSTAL CENTER
LOS ANGELES, CA 90009
(SPACE DEFENSE SYSTEMS)
01CY ATTN SZJ

STRATEGIC AIR COMMAND/XPFS
OFFUTT AFB, NB 68113
01CY ATTN XPFS MAJ B. STEPHAN
01CY ATTN ADWATE MAJ BRUCE BAUER
01CY ATTN NRT
01CY ATTN DOK CHIEF SCIENTIST

SAMSO/SK
P. O. BOX 92960
WORLDWAY POSTAL CENTER
LOS ANGELES, CA 90009
01CY ATTN SKA (SPACE COMM SYSTEMS) M. CLAVIN

SAMSO/MN
NORTON AFB, CA 92409
(MINUTEMAN)
01CY ATTN MNNL LTC KENNEDY

COMMANDER
ROME AIR DEVELOPMENT CENTER, AFSC
HANSCOM AFB, MA 01731
01CY ATTN EEP A. LORENTZEN

DEPARTMENT OF ENERGY
ALBUQUERQUE OPERATIONS OFFICE
P. O. BOX 5400
ALBUQUERQUE, NM 87115
01CY ATTN DOC CON FOR D. SHERWOOD

DEPARTMENT OF ENERGY
LIBRARY ROOM G-042
WASHINGTON, D.C. 20545
01CY ATTN DOC CON FOR A. LABOWITZ

EG&G, INC.
LOS ALAMOS DIVISION
P. O. BOX 809
LOS ALAMOS, NM 85544
01CY ATTN DOC CON FOR J. BREEDLOVE

UNIVERSITY OF CALIFORNIA
LAWRENCE LIVERMORE LABORATORY
P. O. BOX 808
LIVERMORE, CA 94550
01CY ATTN DOC CON FOR TECH INFO DEPT
01CY ATTN DOC CON FOR L-389 R. OTT
01CY ATTN DOC CON FOR L-31 R. HAGER
01CY ATTN DOC CON FOR L-46 F. SEWARD

LOS ALAMOS SCIENTIFIC LABORATORY
P. O. BOX 1663
LOS ALAMOS, NM 87545
01CY ATTN DOC CON FOR J. WOLCOTT
01CY ATTN DOC CON FOR R. F. TASCHEK
01CY ATTN DOC CON FOR E. JONES
01CY ATTN DOC CON FOR J. MALIK
01CY ATTN DOC CON FOR R. JEFFRIES
01CY ATTN DOC CON FOR J. ZINN
01CY ATTN DOC CON FOR P. KEATON
01CY ATTN DOC CON FOR D. WESTERVELT

SANDIA LABORATORIES
P. O. BOX 5800
ALBUQUERQUE, NM 87115
01CY ATTN DOC CON FOR J. MARTIN
01CY ATTN DOC CON FOR W. BROWN
01CY ATTN DOC CON FOR A. THORNBROUGH
01CY ATTN DOC CON FOR T. WRIGHT
01CY ATTN DOC CON FOR D. DAHLGREN
01CY ATTN DOC CON FOR 3141
01CY ATTN DOC CON FOR SPACE PROJECT DIV

SANDIA LABORATORIES
LIVERMORE LABORATORY
P. O. BOX 969
LIVERMORE, CA 94550
01CY ATTN DOC CON FOR B. MURPHEY
01CY ATTN DOC CON FOR T. COOK

OFFICE OF MILITARY APPLICATION
DEPARTMENT OF ENERGY
WASHINGTON, D.C. 20545
01CY ATTN DOC CON FOR D. GALE

OTHER GOVERNMENT

CENTRAL INTELLIGENCE AGENCY
ATTN RD/SI, RM 5G48, HQ BLDG
WASHINGTON, D.C. 20505
01CY ATTN OSI/PSID RM 5F 19

DEPARTMENT OF COMMERCE
NATIONAL BUREAU OF STANDARDS
WASHINGTON, D.C. 20234
(ALL CORRES: ATTN SEC OFFICER FOR)
01CY ATTN R. MOORE

INSTITUTE FOR TELECOM SCIENCES
NATIONAL TELECOMMUNICATIONS & INFO ADMIN
BOULDER, CO 80303
01CY ATTN A. JEAN (UNCLASS ONLY)
01CY ATTN W. UTLAUT
01CY ATTN D. CROMBIE
01CY ATTN L. BERRY

NATIONAL OCEANIC & ATMOSPHERIC ADMIN
ENVIRONMENTAL RESEARCH LABORATORIES
DEPARTMENT OF COMMERCE
BOULDER, CO 80302
01CY ATTN R. GRUBB
01CY ATTN AERONOMY LAB G. REID

DEPARTMENT OF DEFENSE CONTRACTORS

AEROSPACE CORPORATION
P. O. BOX 92957
LOS ANGELES, CA 90009
01CY ATTN I. GARFUNKEL
01CY ATTN T. SALMI
01CY ATTN V. JOSEPHSON
01CY ATTN S. BOWER
01CY ATTN N. STOCKWELL
01CY ATTN D. OLSEN

01CY ATTN SMFA FOR PWW

ANALYTICAL SYSTEMS ENGINEERING CORP
5 OLD CONCORD ROAD
BURLINGTON, MA 01803
01CY ATTN RADIO SCIENCES

BERKELEY RESEARCH ASSOCIATES, INC.
P. O. BOX 983
BERKELEY, CA 94701
01CY ATTN J. WORKMAN

BOEING COMPANY, THE
P. O. BOX 3707
SEATTLE, WA 98124
01CY ATTN G. KEISTER
01CY ATTN D. MURRAY
01CY ATTN G. HALL
01CY ATTN J. KENNEY

CALIFORNIA AT SAN DIEGO, UNIV OF
P.O.Box 6049
San Diego, CA 92106

BROWN ENGINEERING COMPANY, INC.
CUMMINGS RESEARCH PARK
HUNTSVILLE, AL 35807
01CY ATTN ROMEO A. DELIBERIS

CHARLES STARK DRAPER LABORATORY, INC.
555 TECHNOLOGY SQUARE
CAMBRIDGE, MA 02139
01CY ATTN D. B. COX
01CY ATTN J. P. GILMORE

COMSAT LABORATORIES
LINTHICUM ROAD
CLARKSBURG, MD 20734
01CY ATTN G. HYDE

CORNELL UNIVERSITY
DEPARTMENT OF ELECTRICAL ENGINEERING
ITHACA, NY 14850
01CY ATTN D. T. FARLEY JR

ELECTROSPACE SYSTEMS, INC.
BOX 1359
RICHARDSON, TX 75080
01CY ATTN H. LOGSTON
01CY ATTN SECURITY (PAUL PHILLIPS)

ESL INC.
495 JAVA DRIVE
SUNNYVALE, CA 94086
01CY ATTN J. ROBERTS
01CY ATTN JAMES MARSHALL
01CY ATTN C. W. PRETTIE

FORD AEROSPACE & COMMUNICATIONS CORP
3939 FABIAN WAY
PALO ALTO, CA 94303
01CY ATTN J. T. MATTINGLEY

GENERAL ELECTRIC COMPANY
SPACE DIVISION
VALLEY FORGE SPACE CENTER
GODDARD BLVD KING OF PRUSSIA
P. O. BOX 8555
PHILADELPHIA, PA 19101
01CY ATTN M. H. BORTNER SPACE SCI LAB

GENERAL ELECTRIC COMPANY
P. O. BOX 1122
SYRACUSE, NY 13201
01CY ATTN F. REIBERT

GENERAL ELECTRIC COMPANY
TEMPO-CENTER FOR ADVANCED STUDIES
816 STATE STREET (P.O. DRAWER QQ)
SANTA BARBARA, CA 93102
01CY ATTN DASIAC
01CY ATTN DON CHANDLER
01CY ATTN TOM BARRETT
01CY ATTN TIM STEPHANS
01CY ATTN WARREN S. KNAPP
01CY ATTN WILLIAM MCNAMARA
01CY ATTN B. GAMBILL
01CY ATTN MACK STANTON

GENERAL ELECTRIC TECH SERVICES CO., INC.
HMES
COURT STREET
SYRACUSE, NY 13201
01CY ATTN G. MILLMAN

GENERAL RESEARCH CORPORATION
SANTA BARBARA DIVISION
P. O. BOX 6770
SANTA BARBARA, CA 93111
01CY ATTN JOHN ISE JR
01CY ATTN JOEL GARBARINO

GEOPHYSICAL INSTITUTE
UNIVERSITY OF ALASKA
FAIRBANKS, AK 99701
(ALL CLASS ATTN: SECURITY OFFICER)
01CY ATTN T. N. DAVIS (UNCL ONLY)
01CY ATTN NEAL BROWN (UNCL ONLY)
01CY ATTN TECHNICAL LIBRARY

GTE SYLVANIA, INC.
ELECTRONICS SYSTEMS GRP-EASTERN DIV
77 A STREET
NEEDHAM, MA 02194
01CY ATTN MARSHAL CROSS

ILLINOIS, UNIVERSITY OF
DEPARTMENT OF ELECTRICAL ENGINEERING
URBANA, IL 61803
01CY ATTN K. YEH

ILLINOIS, UNIVERSITY OF
107 COBLE HALL
801 S. WRIGHT STREET
URBANA, IL 60680
(ALL CORRES ATTN SECURITY SUPERVISOR FOR)
01CY ATTN K. YEH

INSTITUTE FOR DEFENSE ANALYSES
400 ARMY-NAVY DRIVE
ARLINGTON, VA 22202
01CY ATTN J. M. AEIN
01CY ATTN ERNEST BAUER
01CY ATTN HANS WOLFHARD
01CY ATTN JOEL BENGSTON

HSS, INC.
2 ALFRED CIRCLE
BEDFORD, MA 01730
01CY ATTN DONALD HANSEN

INTL TEL & TELEGRAPH CORPORATION
500 WASHINGTON AVENUE
NUTLEY, NJ 07110
01CY ATTN TECHNICAL LIBRARY

JAYCOR
1401 CAMINO DEL MAR
DEL MAR, CA 92014
01CY ATTN S. R. GOLDMAN

JOHNS HOPKINS UNIVERSITY
APPLIED PHYSICS LABORATORY
JOHNS HOPKINS ROAD
LAUREL, MD 20810
01CY ATTN DOCUMENT LIBRARIAN
01CY ATTN THOMAS POTEMRA
01CY ATTN JOHN DASSOULAS

LOCKHEED MISSILES & SPACE CO INC
P. O. BOX 504
SUNNYVALE, CA 94088
01CY ATTN DEPT 60-12
01CY ATTN D. R. CHURCHILL

LOCKHEED MISSILES AND SPACE CO INC
3251 HANOVER STREET
PALO ALTO, CA 94304
01CY ATTN MARTIN WALT DEPT 52-10
01CY ATTN RICHARD G. JOHNSON DEPT 52-12
01CY ATTN W. L. IMHOF DEPT 52-12

KAMAN SCIENCES CORP
P. O. BOX 7463
COLORADO SPRINGS, CO 80933
01CY ATTN T. MEAGHER

LINKABIT CORP
10453 ROSELLE
SAN DIEGO, CA 92121
01CY ATTN IRWIN JACOBS

M.I.T. LINCOLN LABORATORY
P. O. BOX 73
LEXINGTON, MA 02173
01CY ATTN DAVID M. TOWLE
01CY ATTN P. WALDRON
01CY ATTN L. LOUGHLIN
01CY ATTN D. CLARK

MARTIN MARIETTA CORP
ORLANDO DIVISION
P. O. BOX 5837
ORLANDO, FL 32805
01CY ATTN R. HEFFNER

MCDONNELL DOUGLAS CORPORATION
5301 BOLSA AVENUE
HUNTINGTON BEACH, CA 92647
01CY ATTN N. HARRIS
01CY ATTN J. MOULE
01CY ATTN GEORGE MROZ
01CY ATTN W. OLSON
01CY ATTN R. W. HALPRIN
01CY ATTN TECHNICAL LIBRARY SERVICES

MISSION RESEARCH CORPORATION
735 STATE STREET
SANTA BARBARA, CA 93101
01CY ATTN P. FISCHER
01CY ATTN W. F. CREVIER
01CY ATTN STEVEN L. GUTSCHE
01CY ATTN D. SAPPENFIELD
01CY ATTN R. BOGUSCH
01CY ATTN R. HENDRICK
01CY ATTN RALPH KILB
01CY ATTN DAVE SOWLE
01CY ATTN F. FAJEN
01CY ATTN M. SCHEIBE
01CY ATTN CONRAD L. LONGMIRE
01CY ATTN WARREN A. SCHLUETER

MITRE CORPORATION, THE
P. O. BOX 208
BEDFORD, MA 01730
01CY ATTN JOHN MORGANSTERN
01CY ATTN G. HARDING
01CY ATTN C. E. CALLAHAN

MITRE CORP
WESTGATE RESEARCH PARK
1820 DOLLY MADISON BLVD
MCLEAN, VA 22101
01CY ATTN W. HALL
01CY ATTN W. FOSTER

PACIFIC-SIERRA RESEARCH CORP
1456 CLOVERFIELD BLVD.
SANTA MONICA, CA 90404
01CY ATTN E. C. FIELD JR

PENNSYLVANIA STATE UNIVERSITY
IONOSPHERE RESEARCH LAB
318 ELECTRICAL ENGINEERING EAST
UNIVERSITY PARK, PA 16802
(NO CLASSIFIED TO THIS ADDRESS)
01CY ATTN IONOSPHERIC RESEARCH LAB

PHOTOMETRICS, INC.
442 MARRETT ROAD
LEXINGTON, MA 02173
01CY ATTN IRVING L. KOFSKY

PHYSICAL DYNAMICS INC.
P. O. BOX 3027
BELLEVUE, WA 98009
01CY ATTN E. J. FREMOUW

PHYSICAL DYNAMICS INC.
P. O. BOX 10367
OAKLAND, CA. 94610
ATTN: A. THOMSON

R & D ASSOCIATES
P. O. BOX 9695
MARINA DEL REY, CA 90291
01CY ATTN FORREST GILMORE
01CY ATTN BRYAN GABBARD
01CY ATTN WILLIAM B. WRIGHT JR
01CY ATTN ROBERT F. LELEVIER
01CY ATTN WILLIAM J. KARZAS
01CY ATTN H. ORY
01CY ATTN C. MACDONALD
01CY ATTN R. TURCO

RAND CORPORATION, THE
1700 MAIN STREET
SANTA MONICA, CA 90406
01CY ATTN CULLEN CRAIN
01CY ATTN ED BEDROZIAN

RIVERSIDE RESEARCH INSTITUTE
80 WEST END AVENUE
NEW YORK, NY 10023
01CY ATTN VINCE TRAPANI

SCIENCE APPLICATIONS, INC.
P. O. BOX 2351
LA JOLLA, CA 92038
01CY ATTN LEWIS M. LINSON
01CY ATTN DANIEL A. HAMLIN
01CY ATTN D. SACHS
01CY ATTN E. A. STRAKER
01CY ATTN CURTIS A. SMITH
01CY ATTN JACK MCDOUGALL

RAYTHEON CO.
528 BOSTON POST ROAD
SUDBURY, MA 01776
01CY ATTN BARBARA ADAMS

Science Applications, Incorporated
1710 Goodridge Drive
McLean, VA 22102
Attn: J. Cockayne

Lockheed Missile & Space Co.,Inc.
Huntsville Research & Engr. Ctr.
4800 Bradford Drive
Huntsville, Alabama 35807
Attn: Dale H. Davis

SRI INTERNATIONAL
333 RAVENSWOOD AVENUE
MENLO PARK, CA 94025
01CY ATTN DONALD NEILSON
01CY ATTN ALAN BURNS
01CY ATTN G. SMITH
01CY ATTN L. L. COBB
01CY ATTN DAVID A. JOHNSON
01CY ATTN WALTER G. CHESNUT
01CY ATTN CHARLES L. RINO
01CY ATTN WALTER JAYE
01CY ATTN M. BARON
01CY ATTN RAY L. LEADABRAND
01CY ATTN G. CARPENTER
01CY ATTN G. PRICE
01CY ATTN J. PETERSON
01CY ATTN R. HAKE, JR.
01CY ATTN V. GONZALES
01CY ATTN D. MCDANIEL

TECHNOLOGY INTERNATIONAL CORP
75 WIGGINS AVENUE
BEDFORD, MA 01730
01CY ATTN W. P. BOQUIST

TRW DEFENSE & SPACE SYS GROUP
ONE SPACE PARK
REDONDO BEACH, CA 90278
01CY ATTN R. K. PLEBUCH
01CY ATTN S. ALTSCHULER
01CY ATTN D. DEE

VISIDYNE, INC.
19 THIRD AVENUE
NORTH WEST INDUSTRIAL PARK
BURLINGTON, MA 01803
01CY ATTN CHARLES HUMPHREY
01CY ATTN J. W. CARPENTER

IONOSPHERIC MODELING DISTRIBUTION LIST
UNCLASSIFIED ONLY

PLEASE DISTRIBUTE ONE COPY TO EACH OF THE FOLLOWING PEOPLE:

ADVANCED RESEARCH PROJECTS AGENCY (ARPA)
STRATEGIC TECHNOLOGY OFFICE
ARLINGTON, VIRGINIA

CAPT. DONALD M. LEVINE

NAVAL RESEARCH LABORATORY
WASHINGTON, D.C. 20375

DR. P. MANGE
DR. R. MEIER
DR. E. SZUSZCZEWICZ - CODE 4127
DR. TIMOTHY COFFEY - CODE 4700 (25 COPIES)
DR. S. OSSAKOW - CODE 4780 (100 COPIES)
DR. J. GOODMAN - CODE 7560

SCIENCE APPLICATIONS, INC.
1250 PROSPECT PLAZA
LA JOLLA, CALIFORNIA 92037

DR. D. A. HAMLIN
DR. L. LINSON
DR. D. SACHS

DIRECTOR OF SPACE AND ENVIRONMENTAL LABORATORY
NOAA
BOULDER, COLORADO 80302

DR. A. GLENN JEAN
DR. G. W. ADAMS
DR. D. N. ANDERSON
DR. K. DAVIES
DR. R. F. DONNELLY

A. F. GEOPHYSICS LABORATORY
L. G. HANSOM FIELD
BEDFORD, MASS. 01730

DR. T. ELKINS
DR. W. SWIDER
MRS. R. SAGALYN
DR. J. M. FORBES
DR. T. J. KENESHEA
DR. J. AARONS

OFFICE OF NAVAL RESEARCH
800 NORTH QUINCY STREET
ARLINGTON, VIRGINIA 22217

DR. H. MULLANEY

COMMANDER
NAVAL ELECTRONICS LABORATORY CENTER
SAN DIEGO, CALIFORNIA 92152

MR. R. ROSE

U. S. ARMY ABERDEEN RESEARCH AND DEVELOPMENT CENTER
BALLISTIC RESEARCH LABORATORY
ABERDEEN, MARYLAND

DR. J. HEIMERL

COMMANDER
NAVAL AIR SYSTEMS COMMAND
DEPARTMENT OF THE NAVY
WASHINGTON, D.C. 20360

DR. T. CZUBA

HARVARD UNIVERSITY
HARVARD SQUARE
CAMBRIDGE, MASS. 02138

DR. M. B. MCELROY
DR. R. LINDZEN

PENNSYLVANIA STATE UNIVERSITY
UNIVERSITY PARK, PENNSYLVANIA 16802

DR. J. S. NISBET
DR. P. R. ROHRBAUGH
DR. D. E. BARAN
DR. L. A. CARPENTER
DR. M. LEE
DR. R. DIVANY
DR. P. BENNETT
DR. E. KLEVANS

UNIVERSITY OF CALIFORNIA, LOS ANGELES
405 HILLGARD AVENUE
LOS ANGELES, CALIFORNIA 90024

DR. F. V. CORONITI
DR. C. KENNEL

UNIVERSITY OF CALIFORNIA, BERKELEY
BERKELEY, CALIFORNIA 94720

DR. M. HUDSON

UTAH STATE UNIVERSITY
4TH N. AND 8TH STREETS
LOGAN, UTAH 84322

DR. P. M. BANKS
DR. R. HARRIS
DR. V. PETERSON
DR. R. MEGILL
DR. K. BAKER

CORNELL UNIVERSITY
ITHACA, NEW YORK 14850

DR. W. E. SWARTZ
DR. R. SUDAN
DR. D. FARLEY
DR. M. KELLEY

NASA
GODDARD SPACE FLIGHT CENTER
GREENBELT, MARYLAND 20771

DR. S. CHANDRA
DR. K. MAEDO

PRINCETON UNIVERSITY
PLASMA PHYSICS LABORATORY
PRINCETON, NEW JERSEY 08540

DR. F. PERKINS
DR. E. FRIEMAN

INSTITUTE FOR DEFENSE ANALYSIS
400 ARMY-NAVY DRIVE
ARLINGTON, VIRGINIA 22202

DR. E. BAUER

UNIVERSITY OF MARYLAND
COLLEGE PARK, MD 20742
DR. K. PAPADOPOULOS
DR. E. OTT

UNIVERSITY OF PITTSBURGH
PITTSBURGH, PA. 15213

DR. N. ZABUSKY
DR. M. BIONDI

DEFENSE DOCUMENTATION CENTER
CAMERON STATION
ALEXANDRIA, VA. 22314

12 COPIES IF OPEN PUBLICATION
OTHERWISE 2 COPIES: 12CY ATTN TC

UNIVERSITY OF CALIFORNIA
LOS ALAMOS SCIENTIFIC LABORATORY
P-10, MS-564
LOS ALAMOS, NEW MEXICO 87545

M. PONGRATZ
D. SIMONS
G. BARASCH
L. DUNCAN

University of California,
San Diego
Dept. of Electrical Engineering
& Computer Sciences
Mail Code C-014
La Jolla, CA 92093

Dr. Henry G. Booker

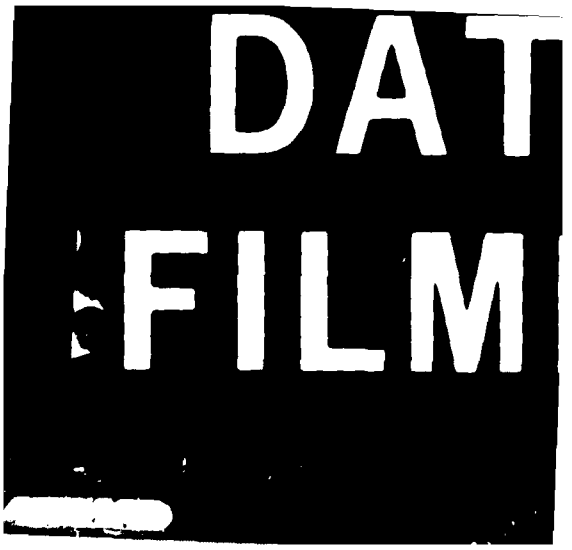
DAT
FILM